S. Schlorholtz

Image Analysis for Evaluating Air Void Parameters of Concrete

June 1998

**Iowa Department
of Transportation**

Final

REPORT

IOWA STATE UNIVERSITY
OF SCIENCE AND TECHNOLOGY

Department of Civil and Construction Engineering

S. Schlorholtz

Image Analysis for Evaluating Air Void Parameters of Concrete

June 1998

Final

REPORT

IOWA STATE UNIVERSITY
OF SCIENCE AND TECHNOLOGY

Iowa Department
of Transportation

Department of Civil and Construction Engineering

TABLE OF CONTENTS

ABSTRACT

This research project investigated the use of image analysis to measure the air void parameters of concrete specimens produced under standard laboratory conditions. The results obtained from the image analysis technique were compared to results obtained from plastic air content tests, Danish air meter tests (also referred to as Air Void Analyzer (AVA) tests), high-pressure air content tests on hardened concrete, and linear traverse tests (as per ASTM C 457). Hardened concrete specimens were sent to three different laboratories for the linear traverse tests. The samples that were circulated to the three labs consisted of specimens that needed different levels of surface preparation. The first set consisted of approximately 18 specimens that had been sectioned from a 4" by 4" by 18" beam using a saw equipped with a diamond blade. These specimens were subjected to the normal sample preparation techniques that were commonly employed by the three different labs (each lab practiced slightly different specimen preparation techniques). The second set of samples consisted of eight specimens that had been ground and polished at a single laboratory. The companion labs were only supposed to retouch the sample surfaces if they exhibited major flaws.

In general, the study indicated that the image analysis test results for entrained air content exhibited good to strong correlation to the average values determined via the linear traverse technique. Specimens ground and polished in a single laboratory and then circulated to the other participating laboratories for the air content determinations exhibited the strongest correlation between the image analysis and linear traverse techniques (coefficient of determination, r-squared=0.96, for n=8). Specimens ground and polished at each of the individual laboratories exhibited considerably more scatter (coefficient of determination, r-squared=0.78, for n=16). The image analysis technique tended to produce low estimates of the specific surface of the voids when compared to the results from the linear traverse method. This caused the image analysis spacing factor calculations to produce larger values than those obtained from the linear traverse tests. The image analysis spacing factors were still successful at distinguishing between the frost-prone test specimens and the other (more durable) test specimens that were studied in this research project.

INTRODUCTION

The slow deterioration of our infrastructure is a continuing problem that has received considerable publicity in the past decade. Continuous efforts must be made to improve the longevity (service life) of portland cement concrete pavement systems because of the tremendous cost of construction and rehabilitation [1].

The purpose of this report is to document the results of research project HR-396 that investigated the use image analysis to quantify the air void parameters of portland cement concrete specimens. The project studied eight different laboratory concrete mixes that were subjected to three different consolidation techniques. The concrete mixtures were dosed with an air-entraining admixture to produce plastic air contents from 3% to 9%. Four of the concrete mixtures contained a Class C fly ash. The goal of the project was to produce a routine image analysis method that could be used to determine the air void parameters of hardened concrete.

BACKGROUND OF AIR VOID ANALYSIS

When field concrete fails to provide a satisfactory service life it is often subjected to petrographic examination to pinpoint the fundamental reason(s) for the poor performance. Petrographic examination generally consists of an evaluation of the integrity and gradation of the coarse and fine aggregates plus an evaluation of the paste fraction of the concrete. In moderate to severe exposure conditions the paste fraction of the concrete typically contains entrained-air voids to help control frost damage. In such instances, the petrographic examination normally includes a technique to determine the air void parameters of the hardened concrete (as per ASTM C 457 [2]).

The test method described in ASTM C 457 uses an optical microscope to determine the air void content, specific surface of the voids and the spacing factor of the voids. These determinations can be made using two different procedures. Procedure A is denoted as the linear traverse method. Procedure B is denoted as the modified point-count method. For the purpose of this report only the details pertaining to the linear traverse procedure will be described. The linear traverse procedure makes use of the stereological principal that the volume fraction of a phase can be estimated by

principle

1

superimposing a line on a plane section of a specimen and then measuring the length of the line that falls within each phase (see Figure 1b). In the actual linear traverse experiment, the length of the various phases (air void, paste or aggregate) are generally recorded by means of a series of mechanical counters that record the number of turns of a screw assembly during the passage of the eyepiece reticule through each phase. Few measurement strategies can be simpler and more efficient than the linear traverse procedure, it does not require any sophisticated measurement equipment and it produces an accurate measurement of the volume of air voids through a series of very simple calculations. In recent years several researchers have suggested a variety of changes to the basic method to allow for a more automated procedure [4-7]. Most of the changes were suggested to make the determinations less labor intensive and less monotonous.

Image analysis has already been used by Iowa researchers to quantify the air content of hardened portland cement concrete [8, 9, 10]; however, these early studies did not have access to modern digital imaging equipment that was procured for Iowa DOT project HR-358 [11]. Also, these preliminary studies failed to produce a routine systematic procedure that could be used to evaluate the air void parameters of concrete. Hence, the goal of this project was to produce a standard operating procedure that could be followed to produce consistent measurements of the air content and void-size distribution in hardened portland cement concrete.

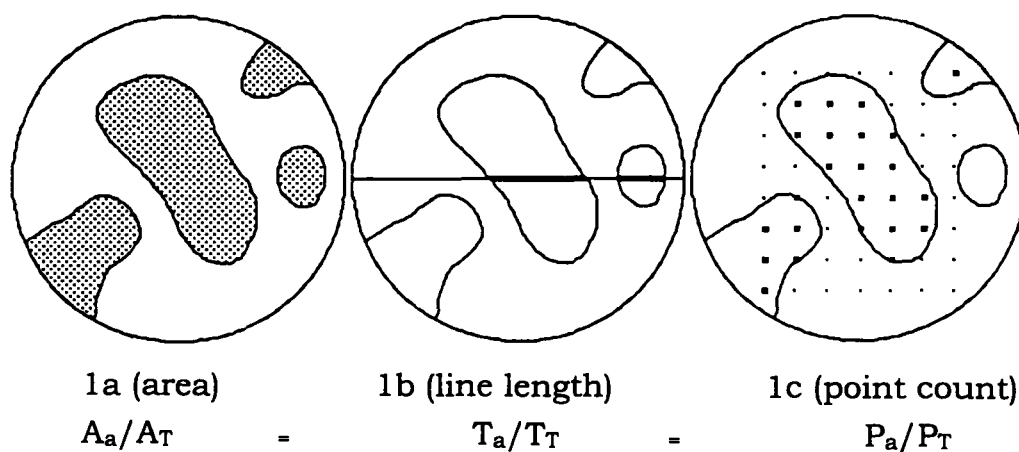| 1a (area)		1b (line length)		1c (point count)
A_a/A_T	$=$	T_a/T_T	$=$	P_a/P_T

Figure 1. Equality of different methods for measuring volume fraction (adapted from [3]). Note, results are equivalent.

Linear Traverse

The linear traverse procedure is described in detail in ASTM C 457 [2]. Excellent summaries of the method are contained in ASTM Special Technical Publications 169B and 169C [12]. Very briefly, in its simplest sense, the test method measures the number of voids (N) and the length of the voids (T_a) encountered while traversing an imaginary line across a test specimen (total length of traverse = T_t). The paste content of the specimen, which is needed for the spacing factor calculations, can be measured by keeping track of the length of the traverse passing through the paste (T_p) or it can be estimated from the concrete batch quantities for any given mix (p = calculated or measured paste content). From these measurements the following parameters can be calculated:

$$\text{Air content (in \%)} = A = 100\ (T_a/T_t) \qquad \text{eqn. 1}$$

$$\text{Average Chord Length} = \bar{l} = T_a/N \qquad \text{eqn. 2}$$

$$\text{Specific Surface} = \alpha = 4/\bar{l} = 4\ N/T_a \qquad \text{eqn. 3}$$

$$\text{Paste-Air Ratio} = p/A = T_p/T_a \qquad \text{eqn. 4}$$

$$\text{Spacing Factor} = \bar{L} = T_p/4N = T_a\,(p)/4\ A\ N \quad \text{for } p/A \leq 4.34 \qquad \text{eqn. 5a}$$

$$\text{Spacing Factor} = \bar{L} = 3/\alpha[1.4(1+p/A)^{1/3}-1] \quad \text{for } p/A > 4.34 \qquad \text{eqn. 5b}$$

If the lengths of the individual air void intercepts are recorded then the chord size distribution can be constructed by plotting a histogram of the data. However, this is not normally done because it is a very tedious process for systems that are not automated.

Image Analysis

It is important to realize that the linear traverse technique is a method of image analysis; however, the analysis is done in a one-dimensional frame of reference. Hence, global assumptions are made prior to the analysis and the output (i.e., results such as air content, specific surface and spacing factor) reference the entire specimen. The image analysis technique used in this

study gathered information from a two dimensional plane. The area was sampled by obtaining a digital image of the field of view. Void area (actually pixel count) was measured rather than chord length. There are several benefits to this type of data acquisition.

The first benefit of image analysis is that it allows one to measure all of the features present in the field of view. This tends to produce much more information (i.e., count more features or directly measure distances) with less effort. This point is illustrated in Figure 2, where a line has been scribed across two hypothetical specimens that contain equally spaced arrays of voids (circles in this instance). This is analogous to the linear traverse method, which employs a one-dimensional traverse across a specimen. The circles have different diameters and it is obvious that the line intersects more large circles than small circles. Image analysis of an image obtained from each specimen would indicate that they both contain circles spaced at roughly equal intervals, but that their diameters were different. These same results would eventually be obtained from the linear traverse procedure but considerably more effort (traverse length or measurement time; however one wants to categorize the effort) would have to be expended to obtain a good sampling of the circles present in specimen#1. Note, that one could simply increase the magnification used to view the circles in specimen#1 so that they appeared on roughly the same scale as those in Figure 2; however, this would also increase the amount of time required to acquire the required information.
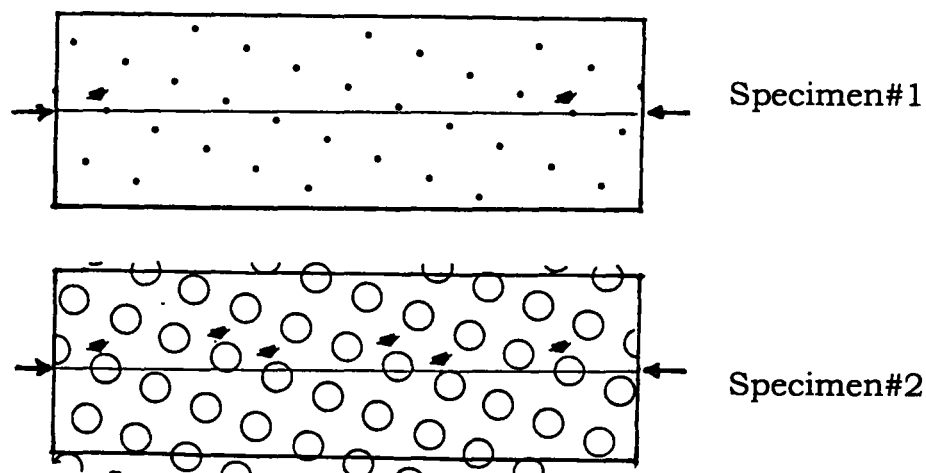

Figure 2. Hypothetical specimens containing equally spaced circles of different sizes. Adapted from [19].

4

Secondly, image analysis allows for a point-wise comparison of each feature in the image. This is arbitrary in the case of the monosized-circles shown in Figure 2; however, a real image of an air-entrained concrete specimen shows how relevant this information can be (see Fig. 3a). Entrained-air voids are not monosized. Their diameters can easily vary over two orders of magnitude (say from 10 to 1000 microns). Point-wise information collection also allows for the easy construction of void-size distribution curves.

Finally, the image analysis technique allows for a higher level of documentation than is currently practiced during normal measurements obtained from the linear traverse method. The digital images can be saved to many different computer formats so they can be archived for future reference or reanalyzed without resorting to another measurement cycle. With the rapidly increasing speed and storage capacity of modern personal computers it seems obvious that image analysis will help to enhance the productivity of petrographic examination of concrete products.

The image analysis procedure that was developed during this project was fairly simplistic. It did not use many of the analytical tools or filters that are commonly packaged in modern image analysis packages. A flowchart depicting the various steps in the process is shown in Figure 4. The experimental details pertaining to the study will be described later in this report. The basic measurement strategy was to obtain a good, high-resolution image from the mortar fraction of the concrete specimen by using a low-vacuum scanning electron microscope (SEM). The SEM image is not required for the image analysis step, any high-quality digital image could be used, as long as the image clearly differentiates between the various features to be quantified. The SEM was employed because it was highly automated, this greatly reduced the level of effort needed for data collection phase of the project. This study focused on the mortar fraction of the specimens because it contained the air voids. Coarse aggregate particles were rejected from the field-of-view via operator intervention. The images were analyzed off-line to produce measurements of void area, perimeter and shape. From these measurements the equivalent void diameter and void (air) content were calculated (along with many other things). The basic output from the analysis was a four page summary of the information based on: (1) a particle size basis; (2) an area fraction basis; (3) histograms depicting void size and area
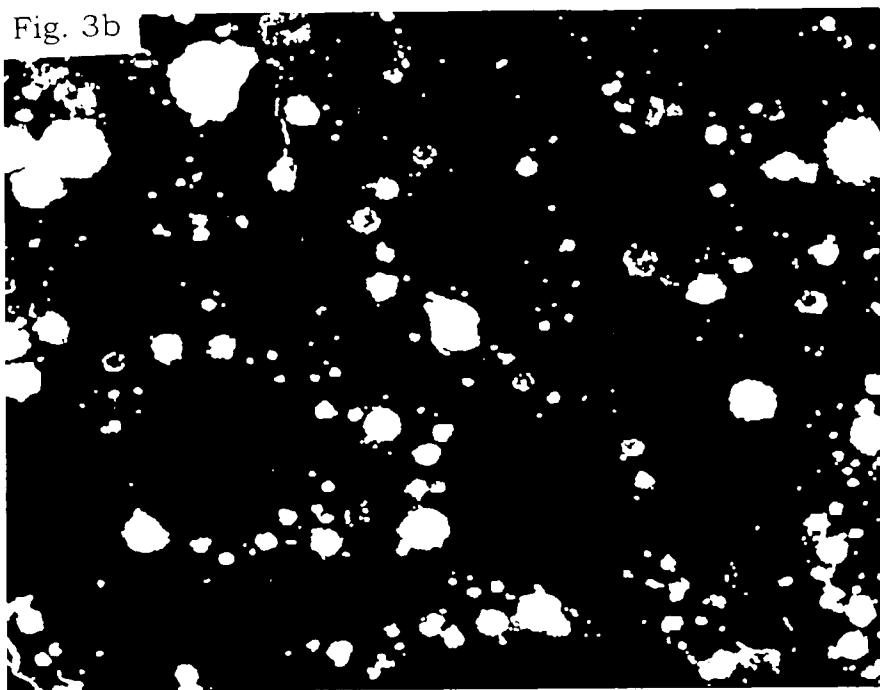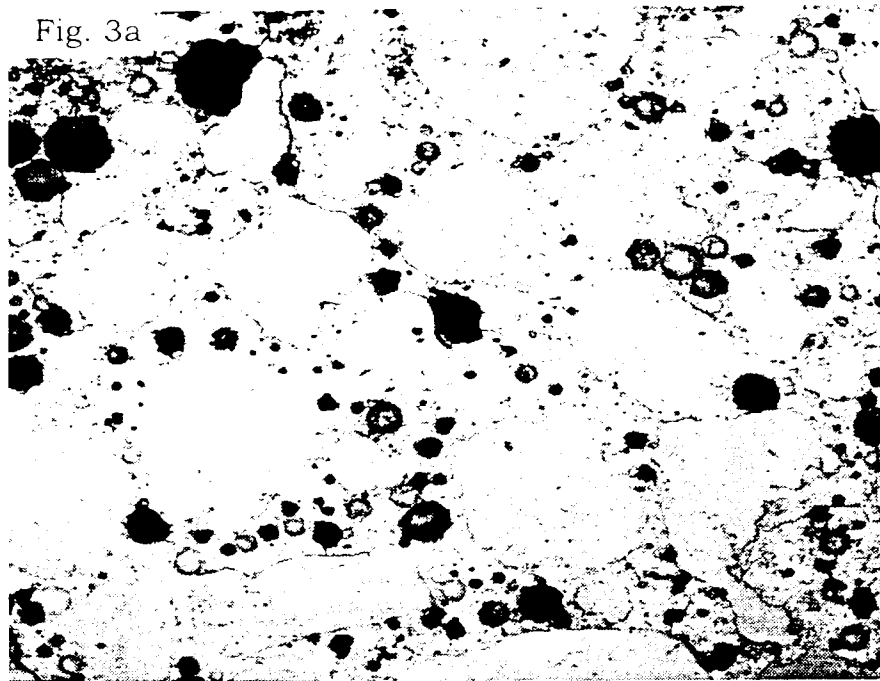
Figure 3.   Digital image of an air-entrained concrete specimen.
Fig. 3a is a backscattered electron image while Fig. 3b
is a binary representation of the gray scale image.

```
        ┌────────────────────────┐                              ┌──────────────────────────┐
        │   Specimen Prep.       │                              │   Image Analysis-1       │
        │  (saw/grind/polish)    │                              │  Create binary image     │
        └───────────┬────────────┘                              │    from raw image        │
                    │                                           └────────────┬─────────────┘
                    ▼                                                        │
        ┌────────────────────────┐                              ┌────────────▼─────────────┐
        │   Attach reference     │                              │   Image Analysis-2       │
        │  standard to specimen  │                              │  Threshold features      │
        └───────────┬────────────┘                              │     of interest          │
                    │                                           └────────────┬─────────────┘
                    ▼                                                        │
        ┌────────────────────────┐                              ┌────────────▼─────────────┐
        │   Put specimen in      │                              │   Image Analysis-3       │
        │   SEM and set          │                              │  Close and open the      │
        │   contrast and         │                              │    binary image          │
        │   brightness by        │                              └────────────┬─────────────┘
        │   using ref. std.      │                                           │
        └───────────┬────────────┘                              ┌────────────▼─────────────┐
                    │                                           │   Image Analysis-4       │
                    ▼                                           │    Fill in holes         │
               ◇ Select ◇                                       └────────────┬─────────────┘
               ◇ areas to ◇                                                  │
               ◇ be imaged ◇                                    ┌────────────▼─────────────┐
                    │                                           │   Image Analysis-5       │
                    ▼                                           │  Measure void area,      │
        ┌────────────────────────┐                              │  perimeter and shape     │
        │   Use AUTOANALYSIS     │                              └────────────┬─────────────┘
        │   to collect images    │                                           │
        └───────────┬────────────┘                              ┌────────────▼─────────────┐
                    │                                           │   Image Analysis-6       │
  ╱Long-term╱  ╱ Store      ╱                                   │  Transfer individual     │
  ╱storage  ╱◀╱ Images on  ╱                                    │  data to EXCEL to        │
  ╱on CD-ROM╱  ╱ hard-drive╱                                    │  create final report     │
                    │                                           └──────────────────────────┘
                    ▼
        ┌────────────────────────┐
        │   Use IMQUANT to       │
        │   analyze the images   │
        └────────────────────────┘
```
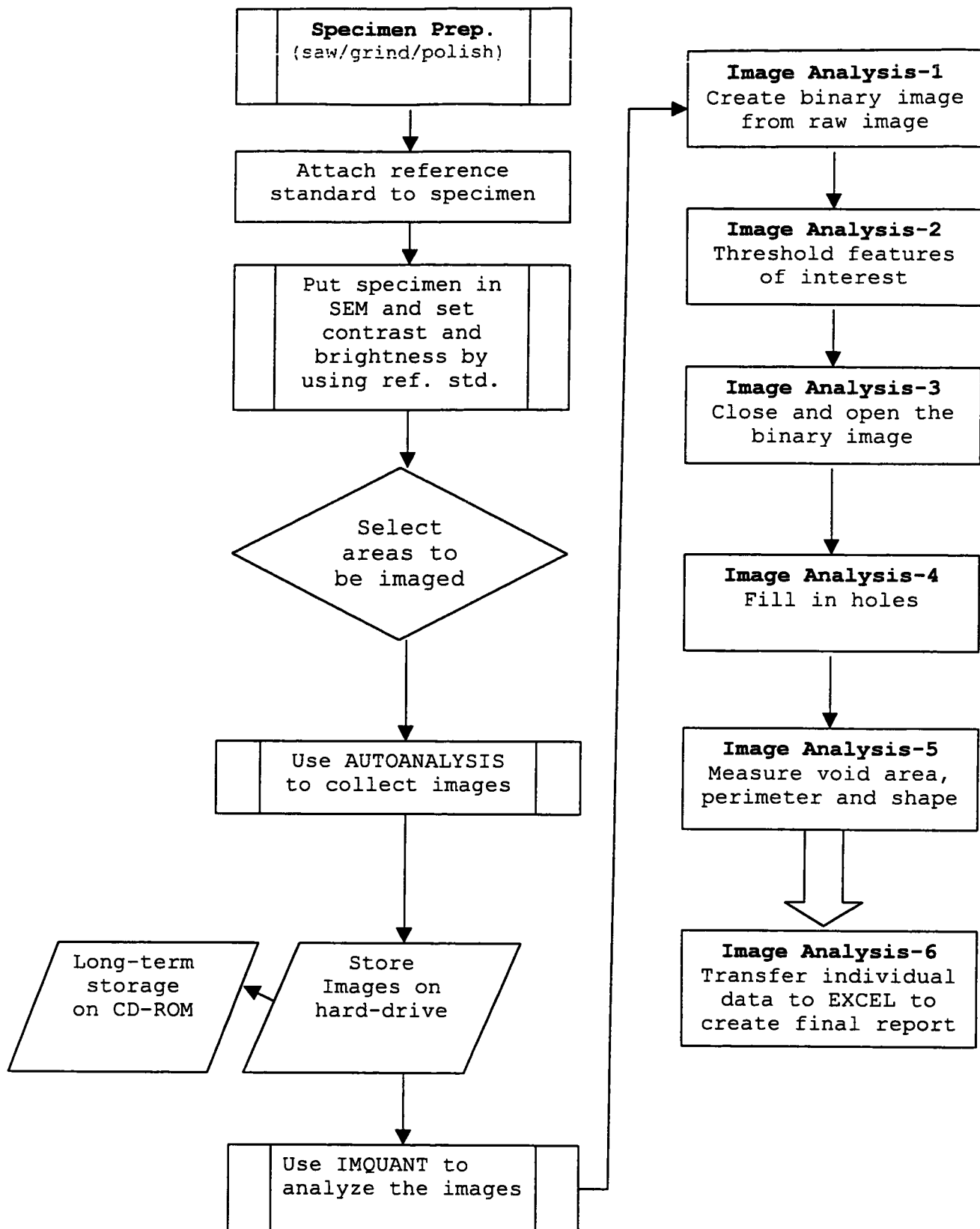
Figure 4.   Flowchart of the measurement and analysis process.

distributions; and (4) a chart depicting the air content on an image-by-image basis. The typical analysis cycle took approximately one hour per specimen (this estimate includes all setup and image measurements plus image analysis but does not include sample cutting, grinding and polishing). Data acquisition and measurement requires about 25 MB of storage space per specimen. It is important to note that the equations listed earlier in this report (see equations 1 through 4) are still applicable to the image analysis procedure, one simply has to replace the measured lengths with the new measurements (areas) and remember that, on a global basis, the average chord length is equal to two-thirds the diameter of the average void. However, there really is no need to resort to global calculations since the point-wise data can be used to obtain image-by-image estimates of any of the desired parameters. After the image-by-image estimates have been calculated they can be combined (averaged) to yield the global estimates, plus an estimate of the statistical uncertainty of the measurements.

EXPERIMENTAL DETAILS

Concrete Mixes

Concrete mixes were formulated using an Iowa Department of Transportation (Ia DOT) C-3 mix design. The nominal batch proportions are summarized in Table 1. Fly ash was substituted for cement on an equivalent mass basis. The dosage of a neutralized-vinsol resin based air-entraining solution (W.R. Grace Daravair) was varied during the study to produce plastic air contents ranging from approximately 3 to 9 percent. The concrete was mixed at the Ia DOT in 1.5-cubic foot batches. The mixing cycle consisted of

Table 1.   Nominal concrete mix proportions used in this study.

Constituent	Absolute Volume	Specific Gravity	Pounds per yd^3
Cement	0.114	3.14	603
Water	0.154	1.00	259
Air	0.060	0.00	--
Fine aggregate	0.302	2.65	1348
Coarse aggregate	0.370	2.65	1652

three minutes of mixing followed by a three-minute rest, followed by two minutes of mixing. The plastic concrete was tested for air content and slump immediately after mixing. The material used for the air content determination was discarded. The material used for the slump test was returned to mixer and remixed for 30 seconds. Then the test specimens were molded using three different consolidation techniques. Beams were molded for the freeze-thaw and linear traverse – image analysis test specimens (nominal size of 4 inches by 4 inches by 18 inches). Cylinders were molded for high-pressure air and compressive strength determinations (4 inches by 8 inches).

The first consolidation technique simply consisted of rodding the plastic concrete into the various molds, no vibration was used in this technique. Hence, this technique was considered to cause little distortion of the air void system. The second consolidation technique used a table vibrator. The molds were vibrated about 15 to 20 seconds prior to striking off the excess concrete from the tops of the molds. This is the normal procedure used at the Ia DOT to produce test specimens for rapid freeze-thaw testing (ASTM C 666 [2]). The third consolidation technique used the table vibrator coupled with an additional vibrator that was inserted into the test specimens (i.e., an insertion probe vibrator) while they were on the vibrator table. The specimens were vibrated for a minimum time of 30 seconds. This technique was expected to cause excessive vibration in the test specimens, and it was done to intentionally distort the air void system.

Tests Conducted On the Concrete Mixes

The plastic concrete mixes were measured for slump, unit weight and air content. The air content was measured using a pressure meter (air pot) in accordance with ASTM C 231 [2]. Specific mixes were also analyzed with the Air Void Analyzer to evaluate the air void parameters of the mixes. The Air Void Analyzer (also known as the Danish Air Meter) was operated by Federal Highway Administration personnel. Details pertaining to the operation and interpretation of the Air Void Analyzer tests can be found elsewhere [13, 14].

The hardened concrete test specimens molded from the various mixes were subjected to the tests listed in Table 2. It is important to note that the specimens molded using the low distortion technique (rodding into the molds) were removed from most of the testing program due to lack of funds. Only the normal and high distortion vibration techniques were subjected to air void

Table 2. Hardened concrete testing program

Test	Increasing level of consolidation energy →		
	Rodded into mold L	Normal Vibration N	Excessive Vibration H
Compressive Strength @ 28-days	No	Yes	No
Freeze-Thaw Test (C 666, method B)	No	Yes	Yes
High-Pressure Air (Ia DOT method)	Yes	Yes	Yes
Linear Traverse (C 457 method)	No (lack of funds)	Yes	Yes
Image Analysis (MARL method)	No (still available)	Yes	Yes

parameter determinations. The low distortion test specimens are still in storage and can be tested if money becomes available.

The freeze-thaw tests were conducted on beams that had been moist-cured for 28-days. After one day of curing in the moist room, the molds were removed from the specimens and then the specimens were immediately submerged in water for the remainder of the curing period. This should have ensured that the specimens were reasonably well saturated prior to the initiation of the freeze-thaw cycling.

Concrete specimens were sent to three different laboratories for the linear traverse tests. The samples were circulated in two different batches. The first set that was circulated consisted of approximately 18 specimens that had been sectioned from a beam using a saw equipped with a diamond blade. This set of specimens was selected in a systematic fashion so that the mean air content of the whole group of specimens should have been approximately constant (assuming of course that the bulk specimens were reasonably homogenous). Each lab also received at least one set of duplicate specimens as an internal check for consistency. Specimens from set 1 were subjected to the normal sample preparation techniques commonly employed at the three different labs (each lab practiced slightly different specimen preparation techniques). The second set of samples consisted of a sub-set of the 18

original specimens described above. This set consisted of eight specimens that had be ground and polished at a single laboratory. The companion labs were instructed to retouch the sample surfaces only if they exhibited major flaws. This set of specimens was selected to contain the whole range of air contents that were observed in this study.

SEM Measurement and Image Analysis

The standard operating procedure (SOP) that was developed during this research project is summarized in Appendix I. The purpose of this section is to give a brief overview of the general procedures, equipment and data acquisition strategies that were used in this study. These features have already been flowcharted in Figure 4.

Sample Preparation Details

The basic sample preparation procedure used in this study was nearly identical to that used in a previous research project [11]. Briefly, it consisted of: (1) coring a section of the concrete beam and then sawing off a section of the core using a Buehler LAPRO slab saw equipped with a diamond blade; (2) rinsing off the propylene glycol; (3) grinding the specimen surface flat using fixed-grit SiC paper and a LECO model VP-50 variable speed grinder/polisher. SiC grit sizes of 180, 320, 600, 800 and 1200 were used throughout this study. The finished specimen was then thoroughly cleaned with water to remove any residual debris, allowed to air dry, and then briefly evacuated in a sputter coater to remove any residual moisture. The specimen surface produced the best images if it was prepared within one day of the image acquisition. Even specimens that were sealed in plastic bags tended to exhibit surfaces that tended to age (loose contrast) rather quickly. Hence, it is normally advantageous to perform a quick surface polish (using 1200-grit paper) just prior to analysis.

Details of Image Collection and Analysis

A Hitachi S-2460N, variable pressure SEM was used to provide the digital images for this project. This SEM was selected because it would accept large specimens (up to 6-inches in diameter) and had a computer controlled specimen stage capable of traversing a four inch specimen. The SEM was

operated at a pressure of 40 Pa and helium was used as the purge gas throughout this study. Experimentation indicated that the optimum working distance should be set as short as possible to obtain the highest quality images. However, due to the possibility of bumping into the backscattered electron detector, it was decided that an 11-mm working distance was a good compromise between image detail and detector safety. Contrast between the air voids and cement paste was maximized at an accelerating voltage of 6 kV.

The SEM was equipped with an Oxford Instruments TETRA backscattered electron detector. Images were acquired using the AUTOSTAGE and AUTOBEAM programs provided by Oxford Instruments [15]. After considerable experimentation it was decided that images obtained at 40X to 50X magnification fulfilled the needs of this project. This, of course, was a compromise between sample throughput and image detail. All images were acquired in high-resolution mode (1024 by 768 pixels) using a dwell-time of 100 microseconds. The AUTOSTAGE software package communicated directly with the DEBEN Research stagecontroller so that fully automated data collection was obtained.

A typical SEM run was initiated by selecting a series of regions (points) of interest from a specimen (20 to 24 different points usually provided about 5000 to 10,000 features for subsequent analysis - this was dependent on the air content of the mortar and the magnification used in the experiment). The regions of interest could be picked in a random fashion or by using a series of preprogrammed stop-points (see Figure 5). Coarse aggregate particles and entrapped air voids (>1mm in diameter) were avoided during the selection process. The preprogrammed stop-points greatly reduced the time needed to select the regions for image collection and they also helped to ensure that the analyst was collecting images from the whole surface of the test specimen. A skilled operator can select 20 areas of interest in approximately 10 to 15 minutes. After the analysis points had been defined, the operator adjusted the contrast and brightness of the TETRA detector to a constant setting by means of a reference standard. This helped to minimize contrast and brightness fluctuations between different images, such fluctuations could complicate the image analysis portion of the process.

Once the images had been collected and saved on the computer hard drive, the image analysis process could begin. The program IMQUANT, which was provided by OXFORD Instruments, was used for this study [15]. The

program uses a script to perform the basic image manipulations used in this study (see the flowchart in Figure 4). The script language provides a wide degree of flexibility for solving image analysis problems. In this instance, since it was desired to measure circular features (i.e., air voids), the script utilized a hexagonal pixel routine to give a better estimate of the area of the voids. Such customizations are relatively quick and painless. The output from IMQUANT consisted of area, perimeter and shape of each individual feature that was isolated in the image. This information was then transferred to Microsoft EXCEL (Version 95 seems to work better than the version packed with OFFICE 97 for some odd reason) for assembling the final (global) estimates of air content and bubble size distribution.
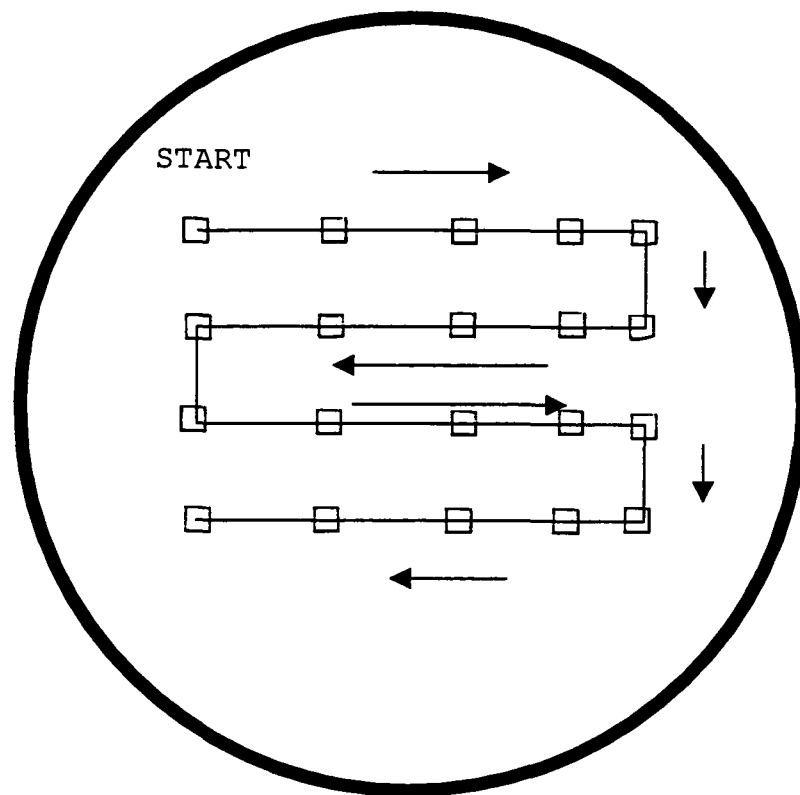
Figure 5.   Procedure used to pick regions of interest on the specimen.

RESULTS AND DISCUSSION

Bulk Materials

The results of chemical and mineralogical analysis of the cement and fly ash used in this study are summarized in Appendix II. The fly ash was a Class C ash and met the appropriate requirements of ASTM C 618 [2]. The portland cement was a Type I cement and met the requirements of ASTM C 150 [16]. The aggregates that were used in the study consisted of a Fort Dodge limestone (coarse aggregate) and a sand from Illinois, just south of Clinton, Iowa (Cordova sand). Both aggregates have been used extensively in previous research projects conducted at the Ia DOT. The normal chemical and mineralogical composition of the aggregates is tabulated in the Iowa DOT aggregate database. Both aggregates exhibit excellent service records when used in field concrete mixes.

Properties of the Plastic Concrete Mixes

Table 3 summarizes the various properties of the concrete mixes that were determined immediately after the mixing process. As expected, the unit weight of the plastic concrete mixtures exhibited a strong correlation to the measured air content (see Figure 6).

The Air Void Analyzer test (AVA) was also conducted on four of the plastic concrete mixes. The results of the AVA tests are summarized in Tables 4 and 5. Overall, the AVA measurements appeared to provide low test results

Table 3.   Plastic concrete properties.

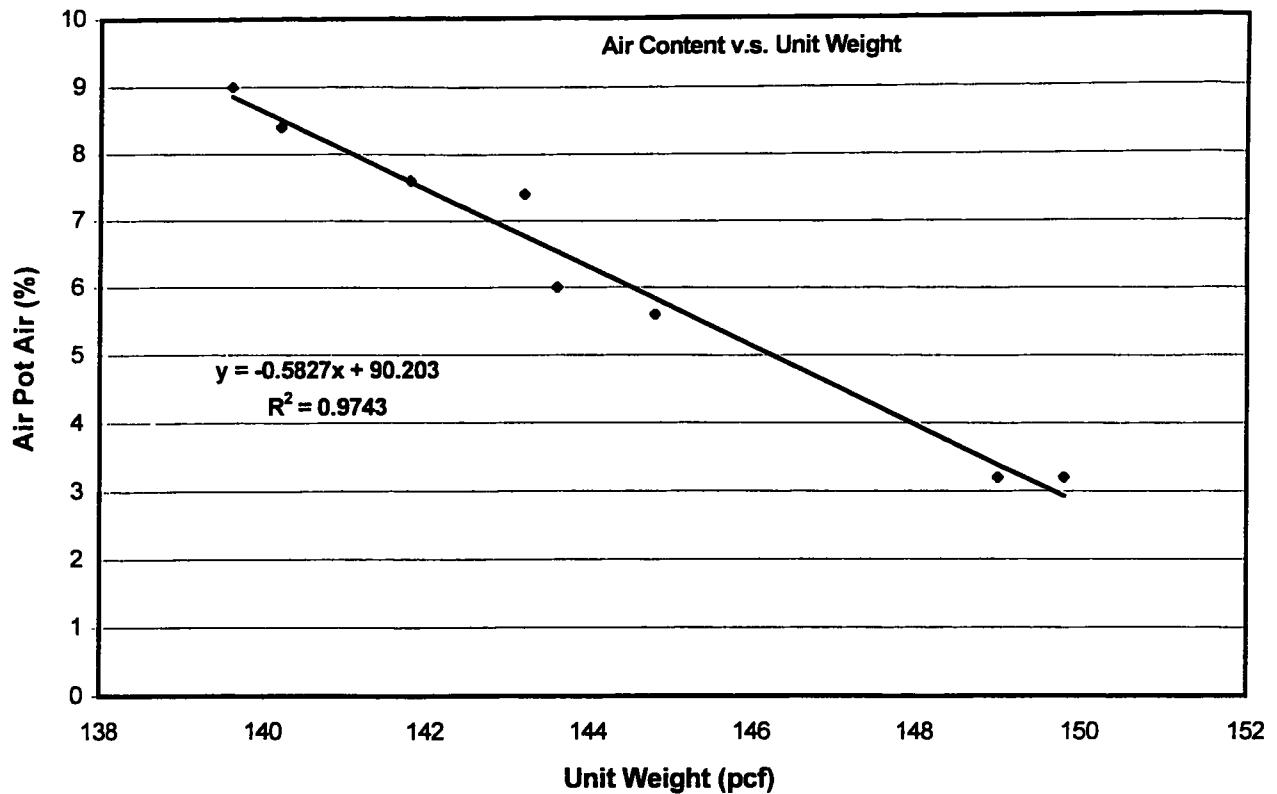| Mix No.	Target Air, %	w/c ratio	Slump (inches)	Unit Weight (pcf)	Air pot (air, %)
1	9	0.40	1.8	140.2	8.4
2-fly ash	9	0.39	2.2	139.6	9.0
3-fly ash	3	0.39	1.5	149.8	3.2
4-fly ash	5	0.39	2.0	144.8	5.6
5	3	0.42	1.8	149.0	3.2
6	5	0.42	2.0	143.6	6.0
7	7	0.42	2.3	141.8	7.6
8-fly ash	7	0.39	2.0	143.2	7.4

Figure 6.   Air content vs unit weight for the mixes in this study.

when compared to the other methods used in this study, this is in agreement with other studies [13]. However, keep in mind that the AVA test was used to assess the plastic properties of the concrete mixes while most of the other tests, with the exception of the air pot test, measure the properties of hardened concrete. Also, the low slump mixes (typically 2 inches or less) coupled with some of the vibration treatments did not lend themselves to easy acquisition of a sample for the AVA testing.

Table 4.   Results of the Air Void Analyzer tests (sample from mixer).

Mix No.	Air Pot Air, %	AVA Air, % (after mixing)	AVA Specific Surface (inches^{-1})	AVA Spacing Factor (inches)
5	3.2	1.7	258	.0300
6	6.0	3.1	538	.0111
7	7.6	3.2	518	.0113
8-fly ash	7.4	3.0	477	.0125

15

Table 5.   Results of the Air Void Analyzer tests (sample after consolidation).

Mix No.	Vibration Level	AVA Air, %	AVA Specific Surface (inches^{-1})	AVA Spacing Factor (inches)
6	High H	Outside range	Outside range	Outside range
7	Normal N	2.2	480	.0144
8-fly ash	Normal N	2.7	397	.0158

Properties of the Hardened Concrete Specimens

The results of the compressive strength and freeze-thaw durability tests are summarized in Table 6. The purpose of the strength testing was simply to see if any drastic errors had been made in the batching process. Overall, all of the mixes exhibited compressive strengths near the nominal mix design level (5000 psi at 28 days), with the exception of the two non-fly ash mixes that contained high air contents (7.6% and 8.4%, respectively). The mixes containing fly ash tended to slightly stronger than the other mixes, this was probably due to the fact that they had lower water-cement ratios.

The purpose of the freeze-thaw testing was to attempt to obtain some information pertaining to the durability of the various concrete mixes. The purpose of entraining air in portland cement concrete is to enhance the durability of the hardened concrete. The test results (see Table 6) clearly indicated that the mixes containing more than 5.6% air (plastic air measured via the air pot) exhibited very good resistance to rapid freezing and thawing. Also, with the exception of the two low-air mixes, it was evident that the various vibration treatments had little influence on the durability of the test specimens. This was not as had been anticipated but it is consistent with the other hardened concrete measurements that will be discussed later in this report.

The two low air mixes (mixes 3 and 5 in Table 3) exhibited poor resistance to cyclical freezing and thawing. Both mixes expanded considerably during the testing and they also exhibited low durability factors (DF in Table 6). In both instances, the test specimen that was subjected to

16

the high vibration treatment exhibited less resistance to freeze-thaw (i.e., higher expansion and lower durability factors). It is currently not clear why mix 3 performed so much better than mix 5; however, mix 3 had a higher compressive strength and it also contained fly ash. These experimental results will be reconsidered later in this report, after the results of the linear traverse and image analysis studies have been reported.

The high-pressure air tests were conducted using the normal procedure developed by the Ia DOT. The results for the low distortion specimens (treatment = L in Table 7) exhibited excellent correlation to the air pot tests which were conducted on the plastic concrete (see Figure 7). It is interesting to note in Table 7, that the medium vibration treatment always produced the highest air contents in the high-pressure air tests. The other two treatments (vibration = L or H) produced similar air contents, although the H treatment often produced the lowest value. This indicates that the vibration treatment did not destroy the entrained air-void system as had been anticipated. The influence of the vibration treatment is illustrated in Figure 8. It is evident that the high vibration treatment produced an excellent agreement (nearly 1:1) between the entrained air content and the total air content of the hardened test specimens. In this instance the entrapped-air voids were assumed to have chord lengths larger than 0.04 inches (1 mm = 1000 microns); the entrained air voids were then assumed to be equal to the total air content minus the entrapped air content. This definition of entrained and entrapped air contents will be used throughout the rest of this report.

Linear Traverse and Image Analysis Measurements

The linear traverse and image analysis hardened air content measurements were only in general agreement with the air contents measured by the air pot (see Table 7). This is in agreement with other studies, which have noted similar trends [12, 13]. It is pertinent to add that the air pot technique uses a filling and compaction procedure that would be most similar to the vibration treatment noted as L in Table 7; however, these specimens were not measured for hardened air content because it was deemed most appropriate to analyze the specimens that were most similar to the freeze-thaw test specimens (i.e., vibration treatments N and H in Table 7).

The goal of this study was to create a test procedure that measures air voids and the various parameters that are commonly used to describe the

Table 6. Results of the compressive strength and freeze-thaw durability tests.

Mix	Air Pot Air cont. (%)	Vibration treatment	Comp. Strength (psi)	DF At 304 cycles	Expansion At 304 cycles (%)	Number of cycles at end of test	RDM at end of test (%)	Expansion At end of test (%)	DF At 1115 cycles
1	8.4	N	4840	97	0.016	1115	98	.022	98
1	8.4	H	-	96	0.012	1115	98	.018	98
2-fly ash	9.0	N	5080	94	0.008	1115	97	.014	97
2-fly ash	9.0	H	-	89*	0.016	1115	84	.031	84
3-fly ash	3.2	N	7480	85	0.077	477	53	.203	24
3-fly ash	3.2	H	-	76	0.151	416	45	.324	21
4-fly ash	5.6	N	6090	92	0.016	1115	92	.038	92
4-fly ash	5.6	H	-	94	0.007	1115	94	.027	94
5	3.2	N	5270	36	0.464	228	38	.464	10
5	3.2	H	-	32	0.606	228	38	.606	9
6	6.0	N	5350	94	0.016	1115	98	.025	98
6	6.0	H	-	94	0.016	1115	96	.031	96
7	7.6	N	4800	99	0.019	1115	98	.033	98
7	7.6	H	-	93	0.018	1115	94	.027	94
8-fly ash	7.4	N	5510	91	0.019	1115	92	.035	92
8-fly ash	7.4	H	-	94	0.017	1115	95	.029	95

*=Sample dropped @ 228 cycles, numbers adjusted

Table 7.　Hardened air content-total air contents (entrapped plus entrained for Labs 1, 2 and 3).

Mix	Air Pot Air, %	Vibration treatment	High-Pressure Air, %	Lab 1 % air, total	Lab 2 % air, total	Lab 3 % air, total	Image Analysis air, %Entrained
1	8.4	L	8.8	-	-	-	-
1	8.4	N	9.5	11.4	6.1	10.0	7.6
1	8.4	H	8.2	9.6	4.5	7.5	5.4
2	9.0	L	9.3	-	-	-	-
2	9.0	N	10.5	14.0	5.4	10.2	8.2
2	9.0	H	7.7	9.9	4.2	7.5	7.1
3	3.2	L	2.8	-	-	-	-
3	3.2	N	3.4	4.7	5.2	3.5	4.4
3	3.2	H	3.1	2.8	3.1	2.3	2.4
4	5.6	L	5.6	-	-	-	-
4	5.6	N	6.6	9.3	5.0	7.2	5.9
4	5.6	H	5.3	7.1	3.5	4.7	4.0
5	3.2	L	2.2	-	-	-	-
5	3.2	N	3.5	4.0	3.9	2.5	4.3
5	3.2	H	2.8	2.4	1.6	1.5	3.2
6	6.0	L	5.8	-	-	-	-
6	6.0	N	6.7	6.6	5.0	6.5	6.2
6	6.0	H	5.5	5.7	4.7	4.5	6.3
7	7.6	L	7.0	-	-	-	-
7	7.6	N	8.3	8.3	5.2	8.1	6.9
7	7.6	H	6.8	7.9	4.5	6.8	5.9
8	7.4	L	6.8	-	-	-	-
8	7.4	N	7.4	9.2	6.1	6.4	6.7
8	7.4	H	6.9	7.5	3.7	6.8	5.4
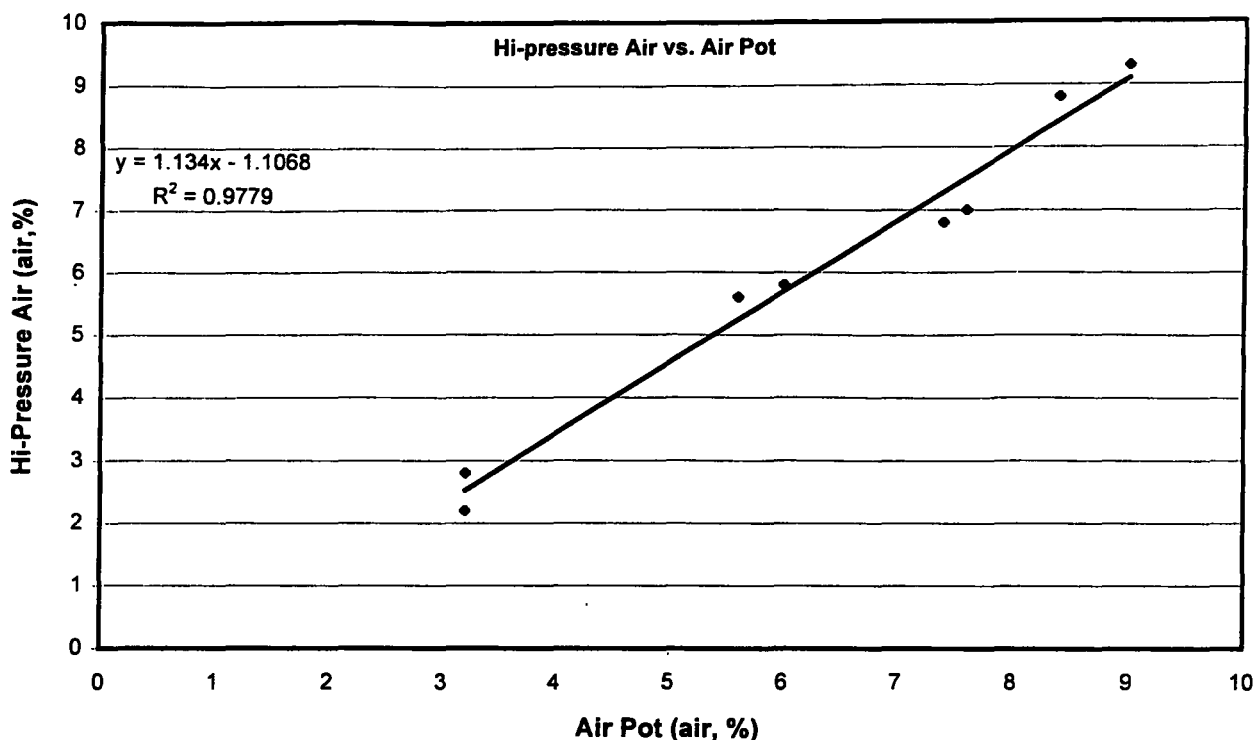
Figure 7.   High-pressure air versus air pot air for the eight mixes.

entrained-air system of portland cement concrete. Hence, it was deemed appropriate to compare the results of the image analysis technique to those obtained from the standard procedure (i.e., linear traverse). Before this could be evaluated, it was decided that the linear traverse method had to be subjected to some scrutiny that would help to define: (1) the difference between duplicate samples determined in any single lab; (2) the differences between multiple labs determining the air content of the same test specimens at similar levels of surface preparation; and finally, (3) the differences between multiple labs determining the air content of similar test specimens using their own surface preparation technique. This was done because the literature makes it very clear that sample preparation is a critical factor in the variability of the results obtained from the linear traverse technique [17, 18].

Similar Specimens Measured at Three Labs

The information from multiple labs determining the air content of similar test specimens has already been presented in Table 7. These specimens were ground and polished at each individual laboratory using
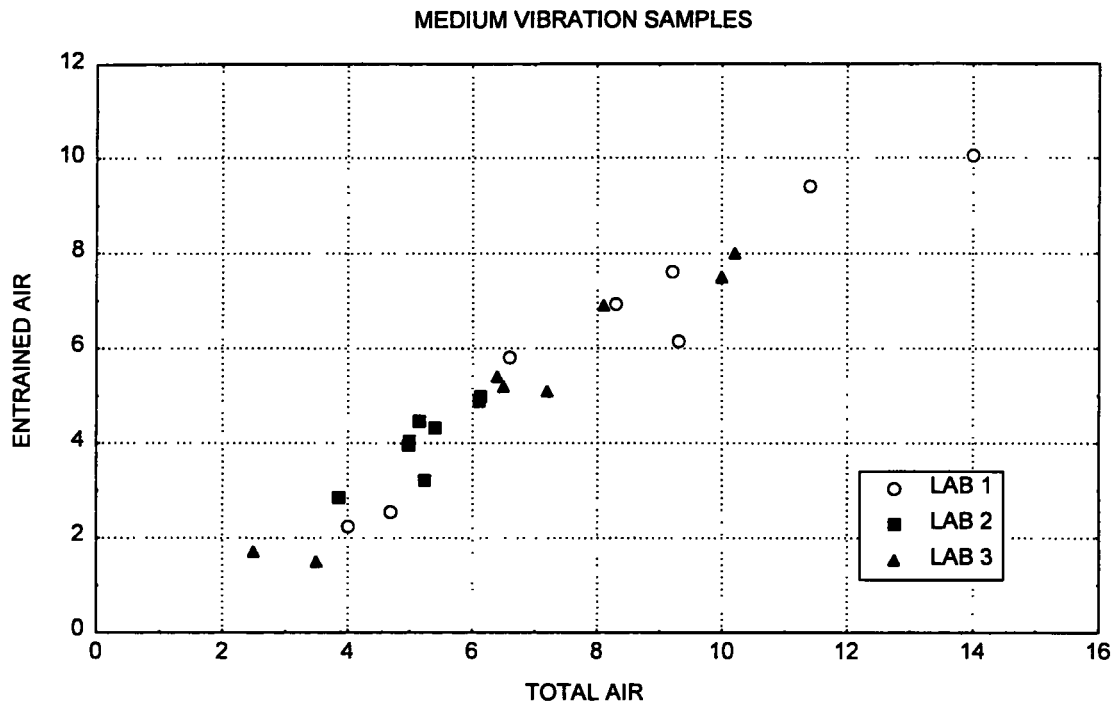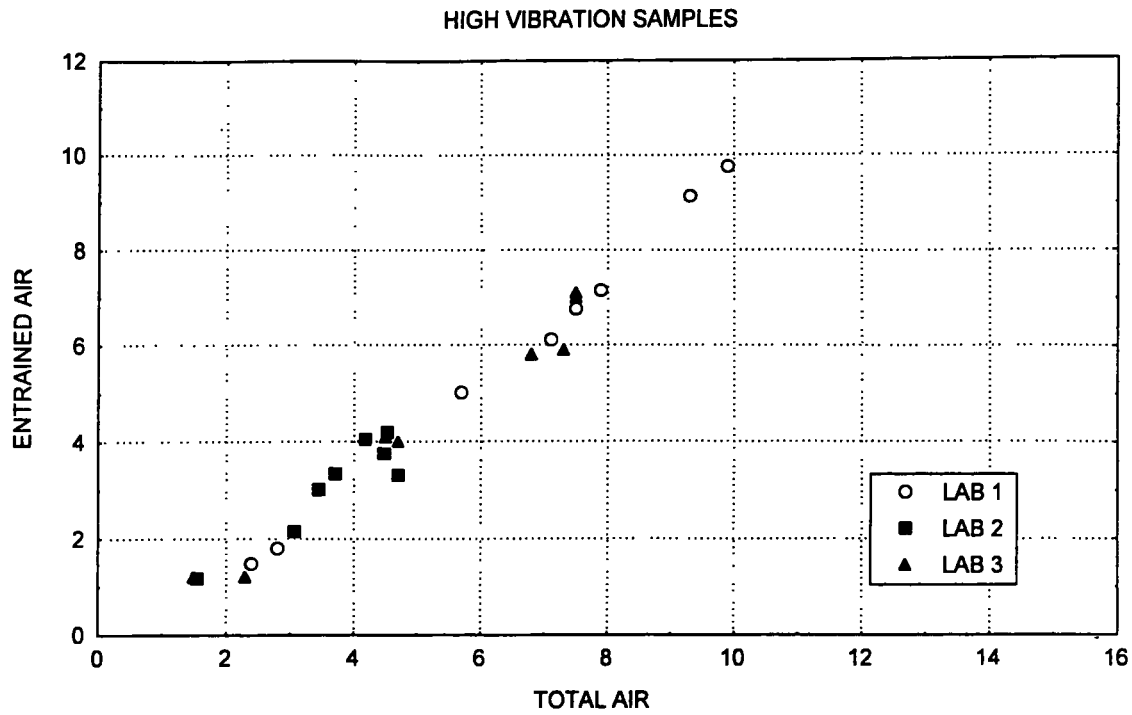
Figure 8.   Influence of vibration on the air content of the specimens.

their own standard operating procedure. To make the information more comparable to the image analysis technique, which only measures entrained air voids, the linear traverse data has been adjusted to remove the air content associated with voids larger than 0.04 inches (1 mm) in diameter. The adjusted air contents, which will be referred to as the entrained-air contents throughout the rest of this report, are summarized in Table 8. Specific surface and spacing factor calculations are summarized in Table 9. The specific surface and spacing factor results are reported as they were reported by the various labs (i.e., they were not corrected for the entrapped air voids).

How well did the labs agree? It depends on how close you want to scrutinize the data. All three labs indicated that the mixes denoted as 3 and 5 should have been prone to freeze-thaw deterioration, this was due to low air contents and high spacing factors. These two mixes did exhibit low durability factors and large expansions during the freeze-thaw testing. However, the labs normally only exhibited general correlation between the various measurements (see Figures 9 and 10). In fact, sometimes the air contents were in poor agreement amongst the various labs (sometimes they were off by nearly a factor of two). The test results from lab 2 appeared to be lower than the other two labs.

Same Specimens With Similar Levels of Surface Preparation

The results of multiple labs determining the air content of the same eight test specimens are summarized in Table 10. These specimens were ground and polished in a single laboratory and then circulated to the remaining labs. Again, total air contents have been converted to entrained-air contents using a maximum void size of 0.04 inches (see Table 11). The results of the specific surface and spacing factor calculations are summarized in Table 12. The spacing factor and specific surface test results are reported exactly as they were summarized by the various labs. Overall, these test results exhibited much less scatter than the previous set of specimens, this was in agreement with previous studies [17, 18]. The correlation between labs was very good (see Figures 11 and 12) and this time lab 2 appeared to produce results more comparable to the other two labs (however, now lab 1 appears to have produced a couple of high values!). Again, all three of the labs clearly identified the two mixes that were susceptible to freeze-thaw deterioration.

Table 8.   Hardened air contents, expressed as entrained-air contents.
Similar samples ground and polished at each individual lab.

Mix	Vibrator Treatment	Lab 1 % air	Lab 2 % air	Lab 3 % air	Image Analysis % air	Image Analysis std. dev.
1	N	9.4	5.0	7.5	7.6	0.69
1	H	9.1	4.2	7.0	5.4	0.47
2	N	10.1	4.3	8.0	8.2	0.59
2	H	9.8	4.1	7.1	7.1	0.49
3	N	2.6	3.2	1.5	4.4	0.88
3	H	1.8	2.2	1.2	2.4	0.69
4	N	6.1	4.0	5.1	5.9	0.64
4	H	6.1	3.0	4.0	4.0	0.48
5	N	2.2	2.8	1.7	4.3	0.76
5	H	1.5	1.2	1.2	3.2	0.71
6	N	5.8	4.0	5.2	6.2	0.62
6	H	5.0	3.3	4.1	6.3	0.52
7	N	6.9	4.5	6.9	6.9	0.59
7	H	7.2	3.8	5.9	5.9	0.57
8	N	7.6	4.9	5.4	6.7	0.61
8	H	6.8	3.4	5.8	5.4	0.47

Table 9.   Specific surface and spacing factor for the samples in Table 8.

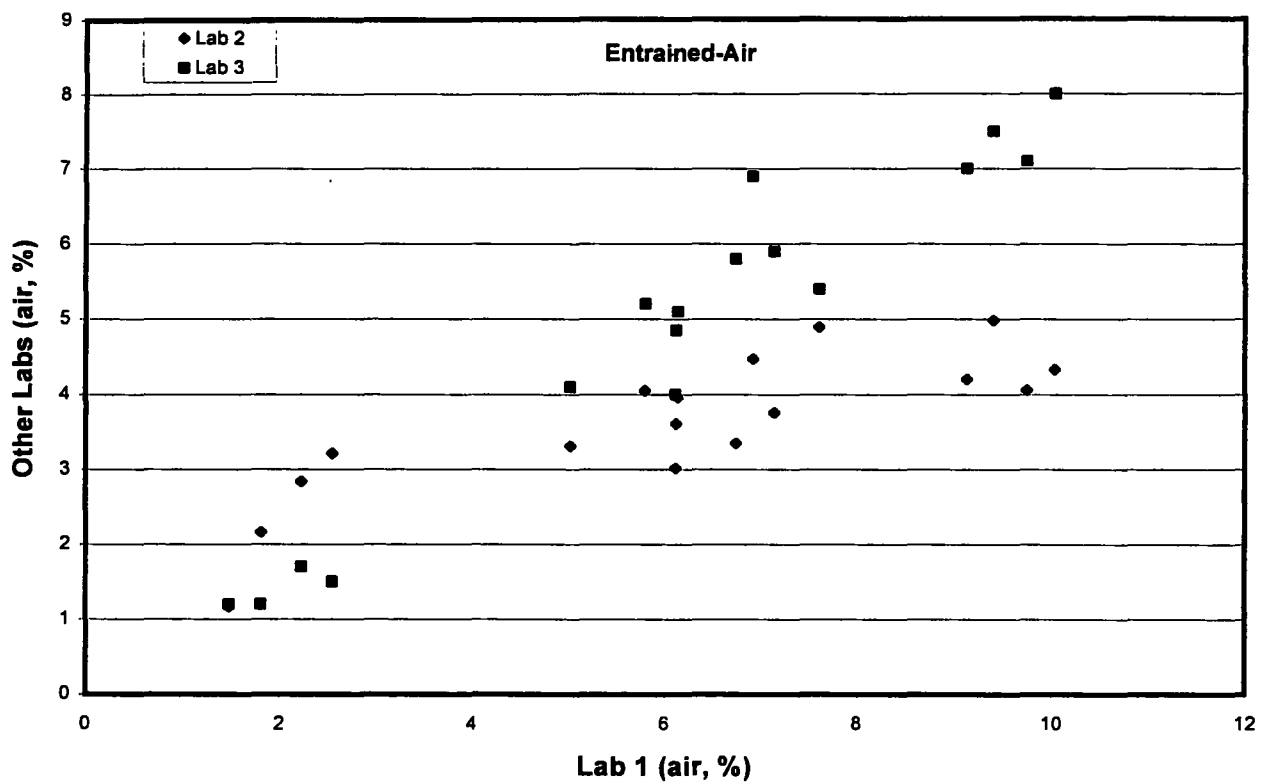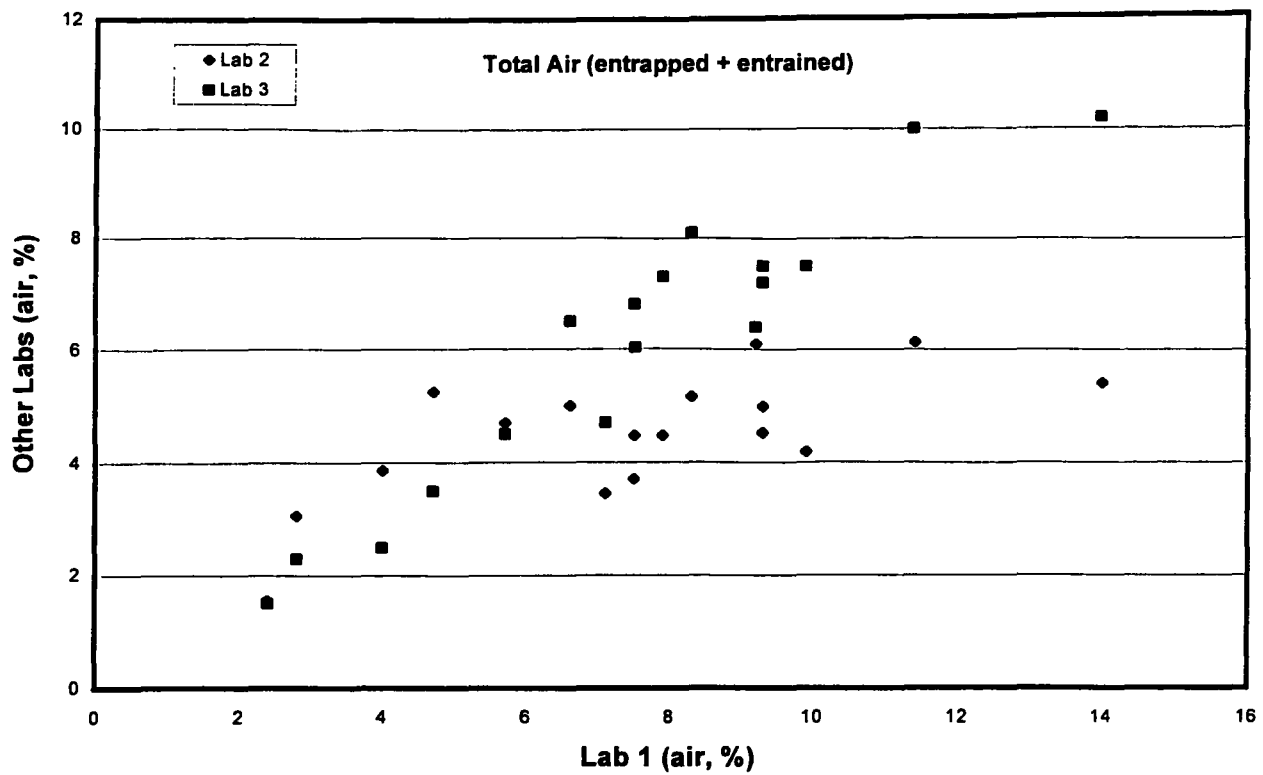| Mix - Vib.	Lab 1 α (inches^{-1})	Lab 1 $\bar{L}$ inches	Lab 2 α (inches^{-1})	Lab 2 $\bar{L}$ inches	Lab 3 α (inches^{-1})	Lab 3 $\bar{L}$ inches
1-N	840	0.003	820	0.006	970	0.003
1-H	1050	0.003	1110	0.005	1310	0.003
2-N	890	0.002	880	0.006	1060	0.004
2-H	1200	0.002	1640	0.003	1260	0.003
3-N	370	0.013	570	0.008	280	0.020
3-H	530	0.012	530	0.010	310	0.022
4-N	680	0.004	810	0.006	830	0.004
4-H	880	0.004	1030	0.006	1130	0.004
5-N	310	0.017	560	0.010	350	0.022
5-H	420	0.016	600	0.014	480	0.017
6-N	800	0.005	870	0.006	950	0.004
6-H	910	0.005	740	0.006	1020	0.005
7-N	870	0.004	910	0.006	970	0.003
7-H	860	0.004	1060	0.005	990	0.004
8-N	870	0.003	990	0.005	1070	0.004
8-H	980	0.004	1320	0.004	1030	0.004

Figure 9. Comparison of linear traverse test results from the three labs. Similar test specimens that were prepared at each lab with their own sample preparation procedure.
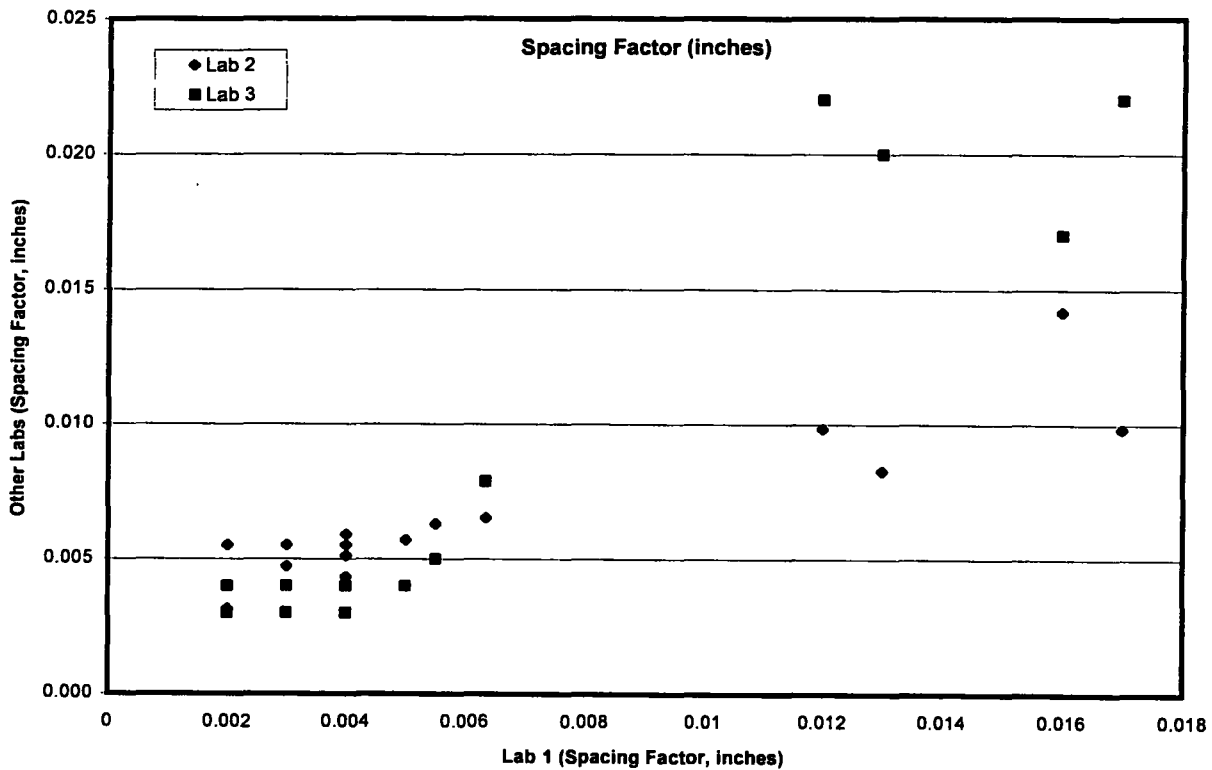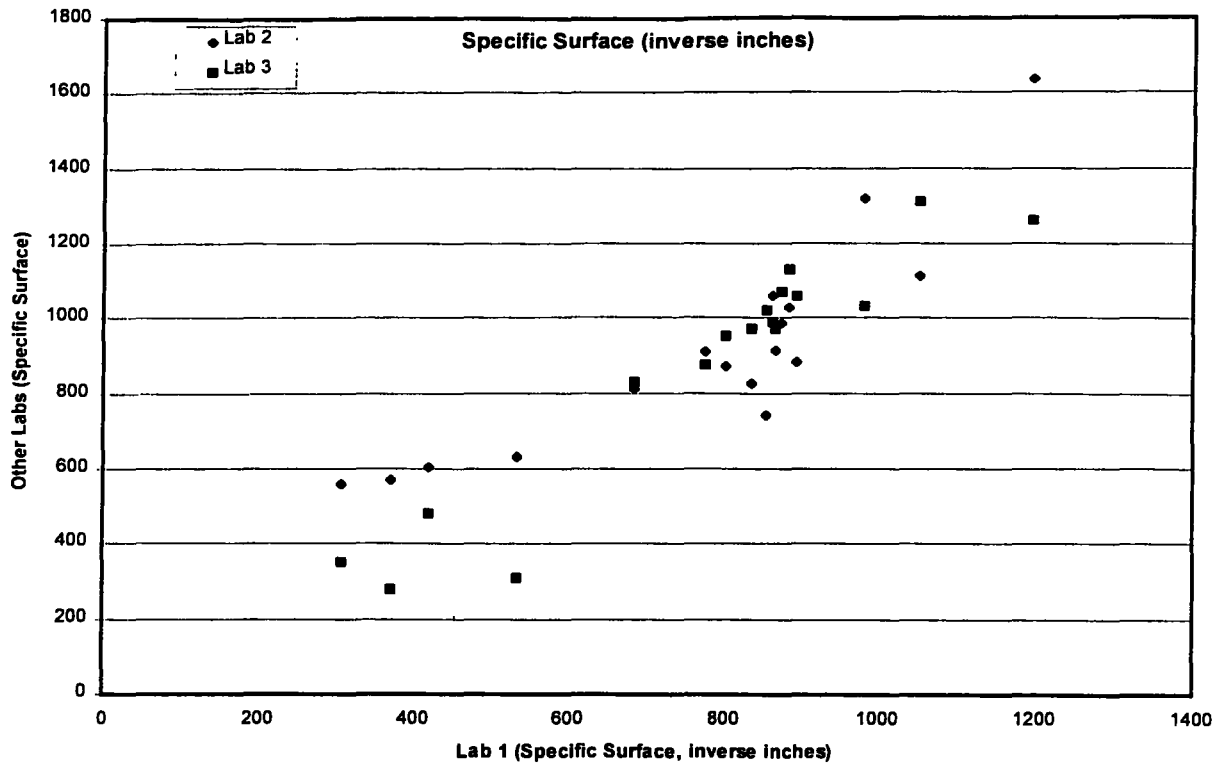
Figure 10.   Comparison of linear traverse test results from the three labs. Similar test specimens that were prepared at each lab with their own sample preparation procedure.

Table 10.   Hardened air contents, expressed as total air contents.
Same samples ground and polished at a single laboratory.

Mix	Vibrator Treatment	Lab 1 % air	Lab 2 % air	Lab 3 % air
1	N	11.4	8.4	7.9
2	N	14.0	10.0	10.0
3	N	4.7	4.7	5.1
3	H	2.0	2.3	2.0
5	N	4.0	5.1	3.6
5	H	2.4	2.4	1.7
6	N	6.6	4.5	5.8
7	N	8.3	5.8	6.9

Table 11.   Hardened air contents, expressed as entrained-air contents.
Same samples ground and polished at a single laboratory.

Mix	Vibrator Treatment	Lab 1 % air	Lab 2 % air	Lab 3 % air	Image Analysis % air	Std Dev. Image Analysis
1	N	9.4	6.1	6.1	6.3	0.49
2	N	10.0	8.2	6.8	7.5	0.52
3	N	2.6	3.0	2.4	2.4	0.62
3	H	1.8	1.0	1.1	2.0	0.65
5	N	2.2	2.8	2.5	3.6	0.64
5	H	1.5	1.7	1.2	2.0	0.56
6	N	5.8	3.8	5.1	4.7	0.41
7	N	6.9	4.5	5.8	6.0	0.47

Table 12.   Specific surface and spacing factors for the second set of samples.
Same samples ground and polished at a single laboratory.

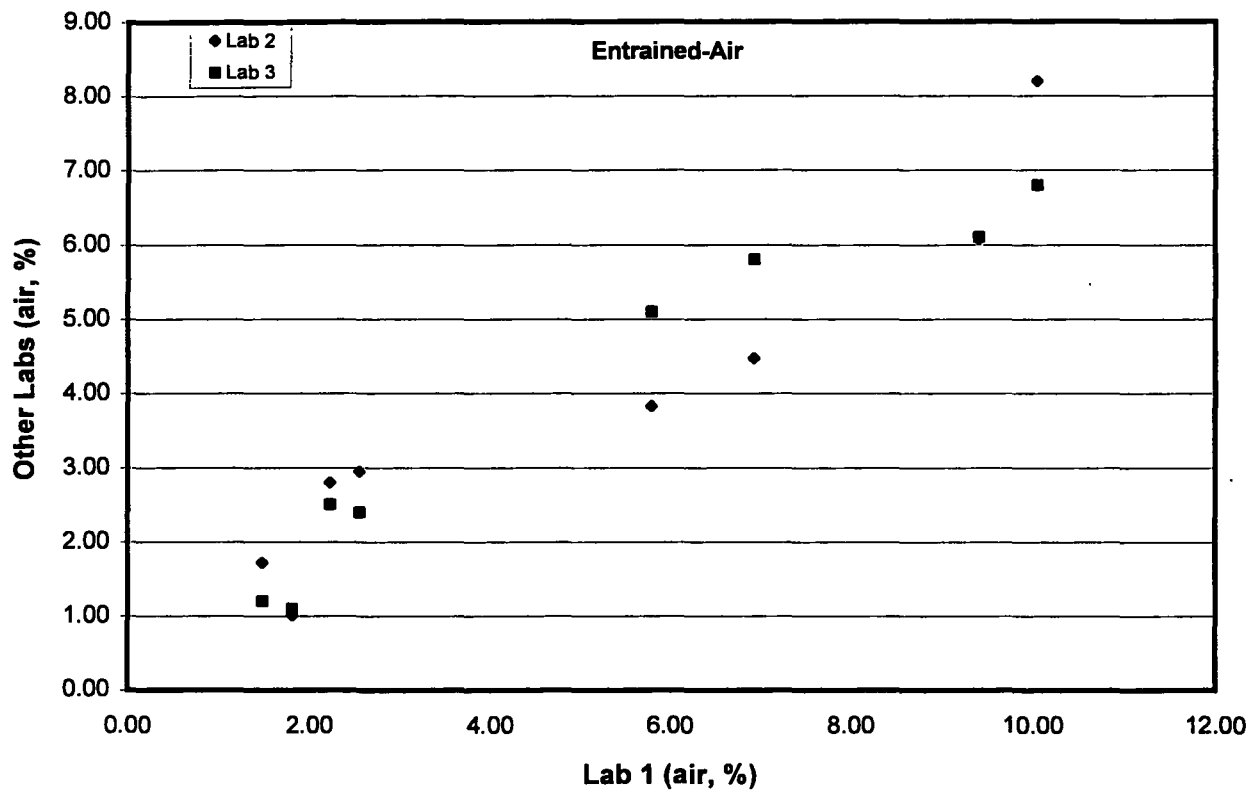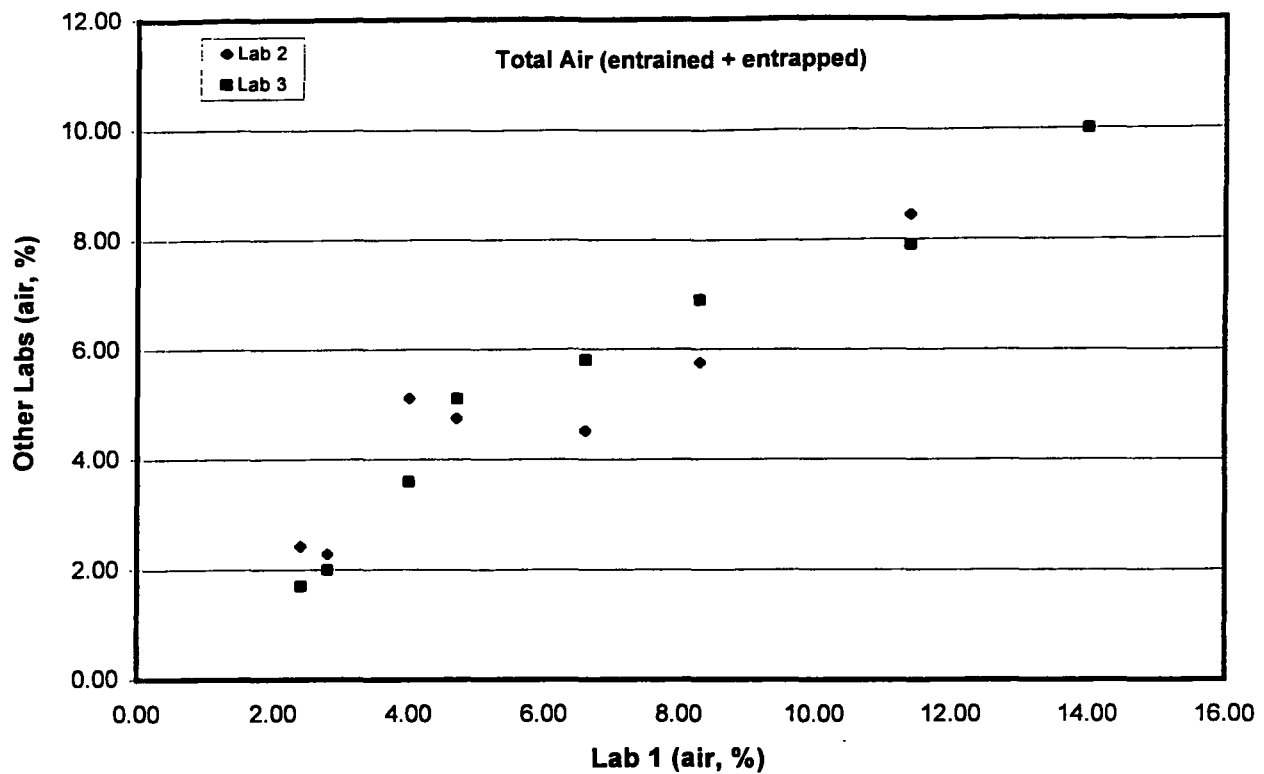| Mix-Vib.-slice	Lab 1 α (inches^{-1})	Lab 1 $\bar{L}$ inches	Lab 2 α (inches^{-1})	Lab 2 $\bar{L}$ inches	Lab 3 α (inches^{-1})	Lab 3 $\bar{L}$ inches
1N-2	836	0.003	917	0.004	930	0.004
2N-3	894	0.002	1101	0.002	750	0.003
3N-1	372	0.013	384	0.012	280	0.018
3H-4	534	0.012	548	0.013	550	0.013
5N-3	307	0.017	394	0.011	320	0.017
5H-2	419	0.016	732	0.009	470	0.017
6N-1	802	0.005	759	0.007	850	0.005
7N-2	867	0.004	924	0.005	910	0.004

Figure 11. Comparison of linear traverse test results from three labs. The same test specimens were prepared in a single lab and then circulated to the other two labs.
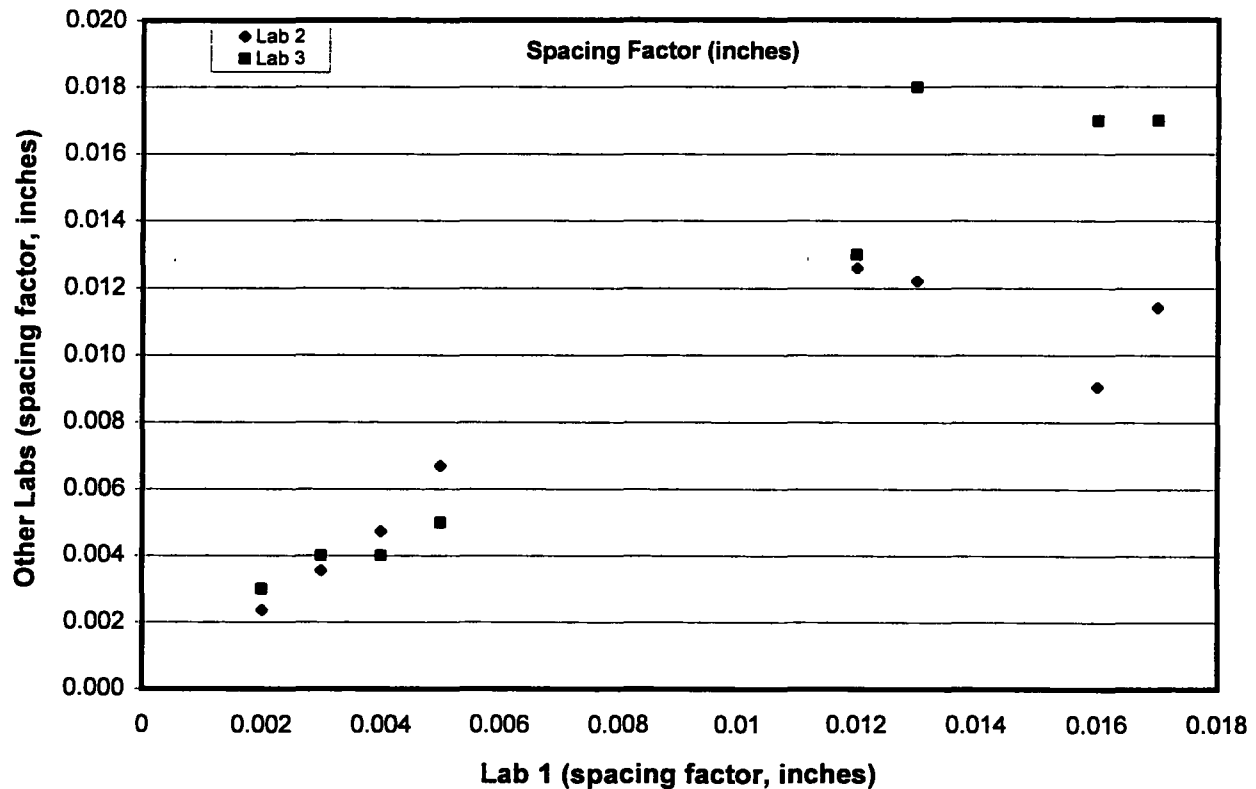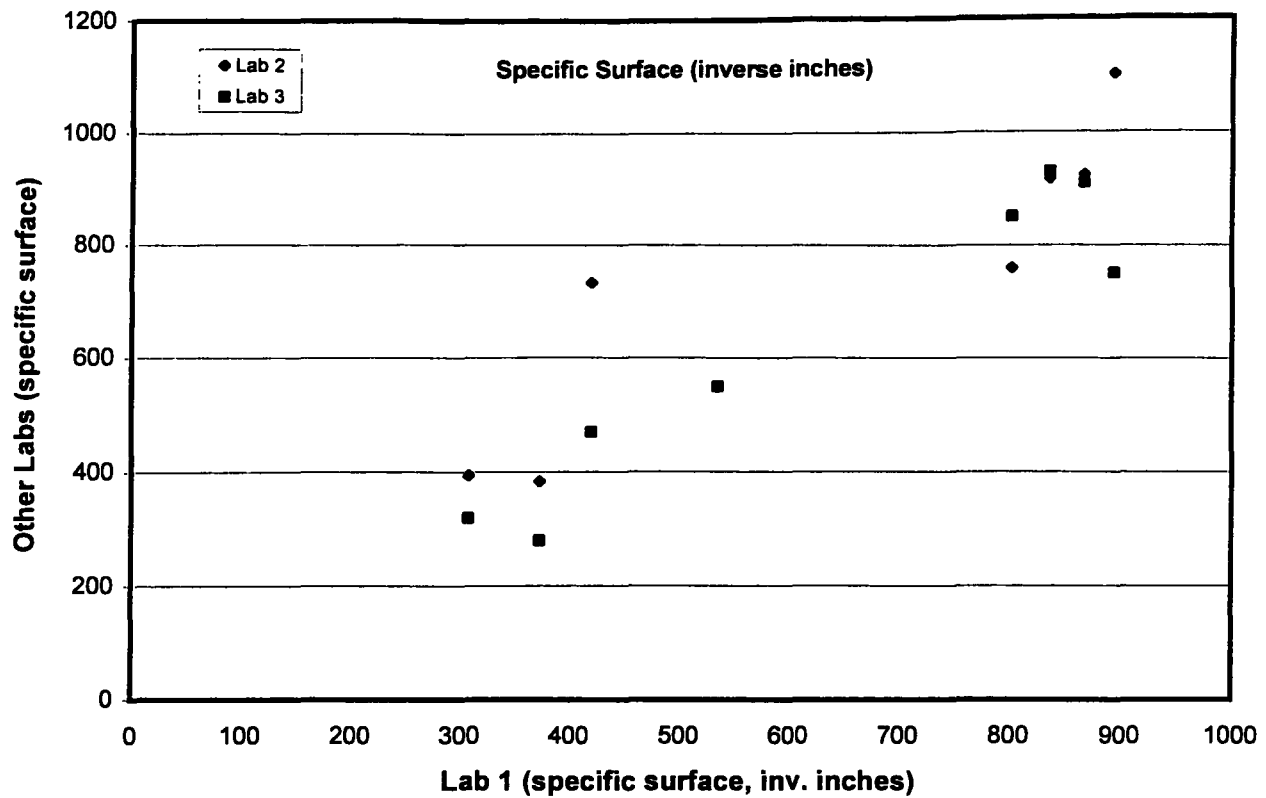
Figure 12. Comparison of linear traverse test results from the three labs. The
same test specimens were prepared in a single lab and then
circulated to the other two labs.

Duplicate Specimens Measured at Different Labs

The results of linear traverse analysis on sets of duplicate test specimens are reported in Table 13. These tests were conducted to evaluate the homogeneity of the beams that were sectioned to create the test specimens. They also give a rough idea of how well duplicate test results should agree when obtained from any single lab, this should reflect the best agreement that could be expected from the tests as they were conducted for this project. Overall, the air content determinations from any single lab were reproducible to about one percent (absolute), the specific surface values to about 10% (relative error), and the spacing factors to about ±0.001 or ±0.002 inches (absolute). All of these results indicated that each lab provided a high level of internal consistency and repeatability for their determinations. The results also indicated that the test specimens were reasonably homogeneous. This suggests that the disagreements between the various testing labs were most likely caused by differences in sample preparation procedures.

Comparison of Image Analysis to Linear Traverse

The whole point of the previous three sections was to set a baseline for evaluating how well one should expect the results from image analysis to compare with those obtained from the linear traverse method. It seems obvious that one should not expect perfect agreement between the two different procedures. However, as a starting point, it seems reasonable to

Table 13. Summary of repeatability tests for the three linear traverse labs. Similar samples ground and polished at each individual lab.

Lab	Sample-Vib.-Slice	Total Air, %	Entrained Air, %	Specific Surface α, (inches^{-1})	Spacing Factor, $\bar{L}$, (inches)
1	6H-3	5.3	4.8	911	0.005
1	6H-4	6.1	5.2	800	0.006
2	7N-3	4.7	3.9	940	0.006
2	7N-4	5.6	5.0	800	0.006
2	6N-2	4.5	3.8	770	0.007
2	6N-4	5.5	4.3	1060	0.004
3	7H-3	7.3	5.9	990	0.004
3	7H-4	6.2	5.6	1230	0.003

compare the results using the same global estimates that were discussed earlier in this report.

Test results for the entrained-air contents determined using the image analysis procedure have already been summarized in Tables 8 and 11. The results of calculations for specific surface and spacing factor are summarized in Tables 14 and 15. The calculations were made using the same basic assumptions that were made for the linear traverse calculations. However, the necessary length measurement needed to calculate specific surface and spacing factor was derived from the area measurements of the voids (which is what was actually measured in the image analysis technique). These values were weighted using the void area to provide a more stable estimate of the mean void diameter. Figures 13 and 14 illustrate the relationship that was observed between the air content determined by image analysis and the air content determined by linear traverse. The top half of each figure depicts the raw data and the bottom half depicts the relationship when the linear traverse test results are averaged together. In either instance the test results appeared

Table 14.   Results of the image analysis procedure for air void parameters. Similar samples ground and polished at the MARL.

Mix	Vibrator Treatment	Specific Surface α, (inches^{-1})	Spacing Factor, $\bar{L}$, (inches)	Image Analysis % air	Std Dev. Image Analysis
1	N	530	0.007	7.6	0.69
1	H	780	0.006	5.4	0.47
2	N	560	0.007	8.2	0.59
2	H	820	0.005	7.1	0.49
3	N	260	0.020	4.4	0.88
3	H	240	0.028	2.4	0.69
4	N	465	0.010	5.9	0.64
4	H	640	0.008	4.0	0.48
5	N	230	0.023	4.3	0.76
5	H	300	0.020	3.2	0.71
6	N	460	0.010	6.2	0.62
6	H	480	0.009	6.3	0.52
7	N	390	0.010	6.9	0.59
7	H	670	0.007	5.9	0.57
8	N	520	0.008	6.7	0.61
8	H	620	0.007	5.4	0.47

Table 15. Results of the image analysis procedure for air void parameters. Same samples ground and polished at a single lab.

Mix	Vibrator Treatment	Specific Surface α, (inches^{-1})	Spacing Factor, $\bar{L}$, (inches)	Image Analysis % air	Std Dev. Image Analysis
1	N	630	0.007	6.3	0.49
2	N	530	0.007	7.5	0.52
3	N	340	0.020	2.4	0.62
3	H	220	0.033	2.0	0.65
5	N	270	0.027	3.6	0.64
5	H	260	0.022	2.0	0.56
6	N	720	0.007	4.7	0.41
7	N	580	0.008	6.0	0.47

to be well correlated (r^2 = 0.96 for the specimens that were ground and polished in a single lab and then circulated for analysis (see Fig. 13), versus r^2 = 0.78 for the other set of test specimens (see Fig. 14). Figure 15 illustrates the relationships that were observed for specific surface and spacing factor. The area-weighting of the mean void size tended to give it some stability but it also caused the specific surface estimates to be lower than those that were obtained from the linear traverse tests. The test results show a good correlation, especially if the two rather high values reported by Lab 2 are ignored. The low specific surface values caused the spacing factor calculations to be larger than those that were reported from the linear traverse tests. This did not influence the meaning of the values it simply changed their magnitude. Spacing factors from the specimens that performed well in the freeze-thaw tests tended to cluster near the bottom, left-hand side of Figure 15; spacing factors for the specimens that failed the test tended to plot in the upper right-hand portion of the graph.

Void-Size Distributions and Concrete Durability

One of the strengths of the image analysis technique is that it simplifies the collection of information that can be used to create void size distribution curves. When the linear traverse technique is used this process is very labor intensive; and hence, such information is usually not collected unless the information has been specifically requested or the linear traverse system has been automated to some extent. It is important to realize that when concrete is sectioned for analysis it is much more probable to cut through a large void
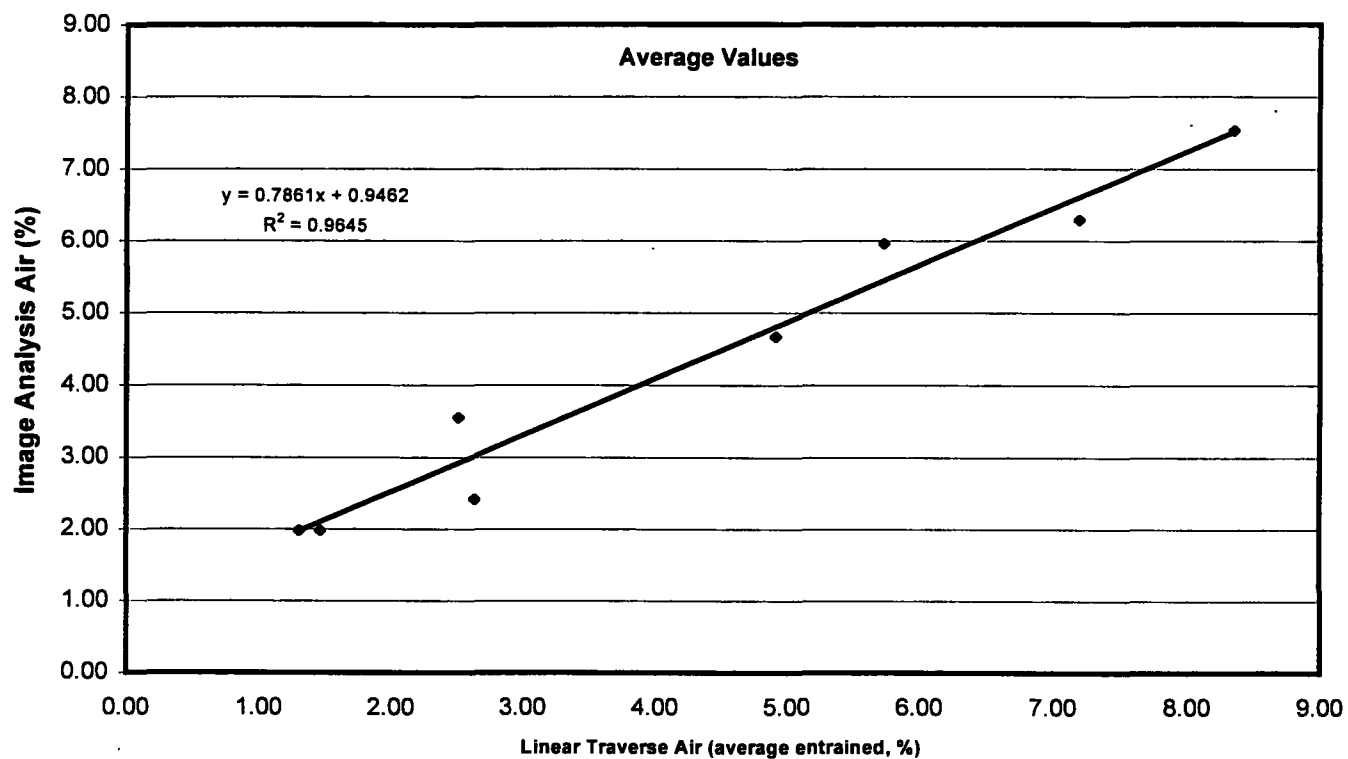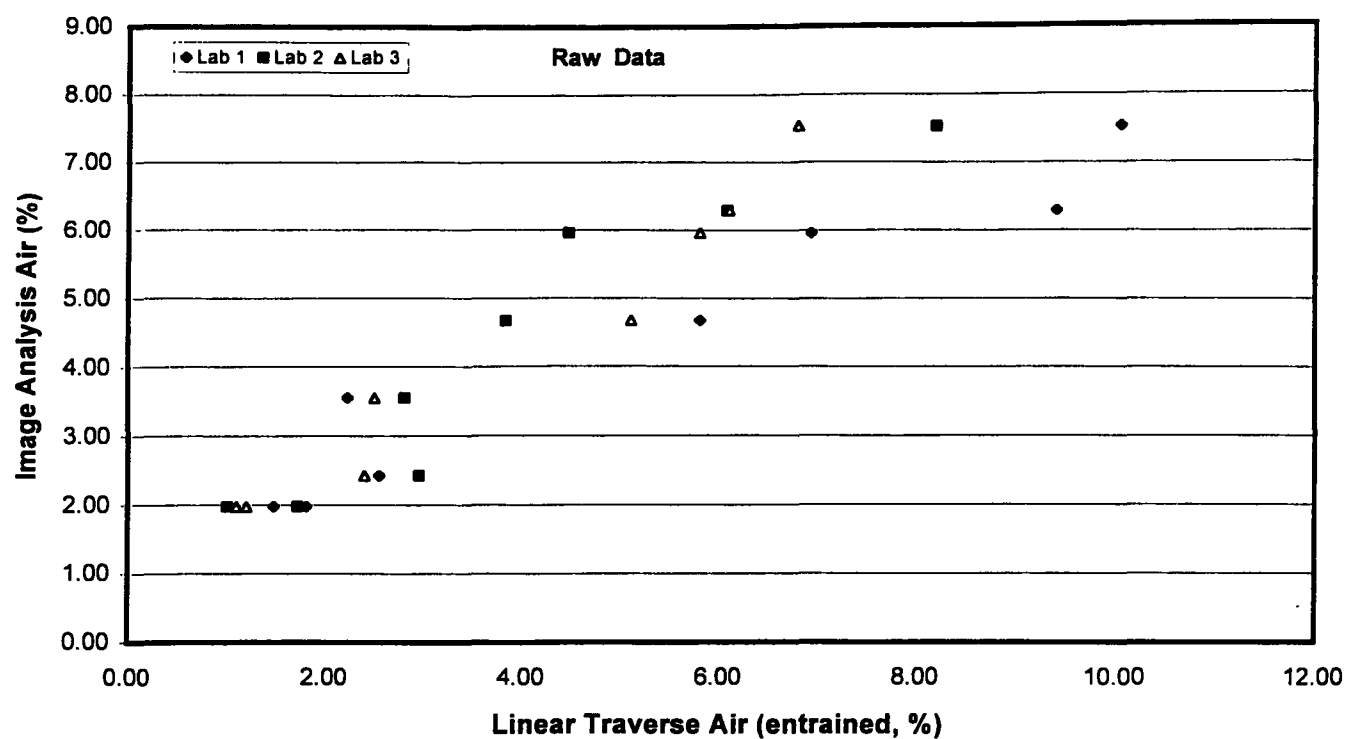
Figure 13.   Comparison of image analysis results to the linear traverse results
             for the specimens that were prepared in a single laboratory.
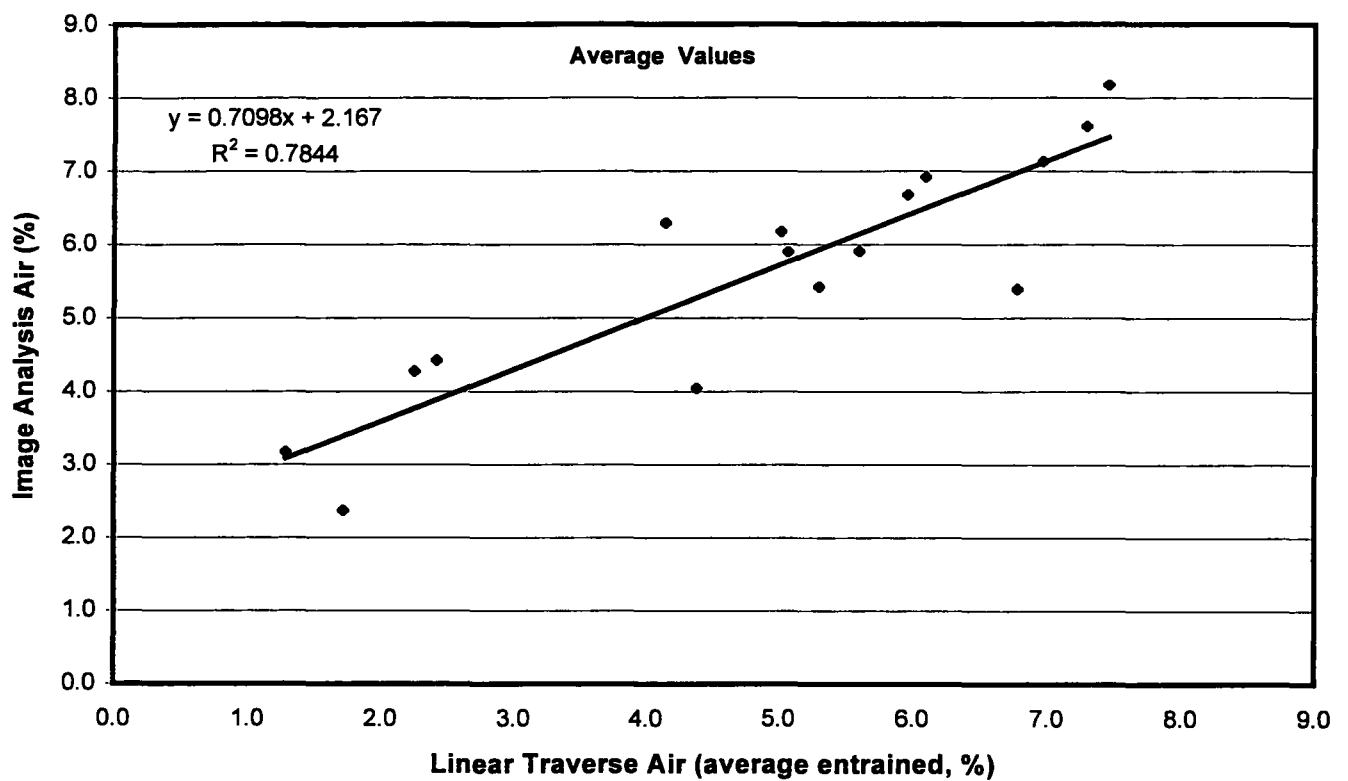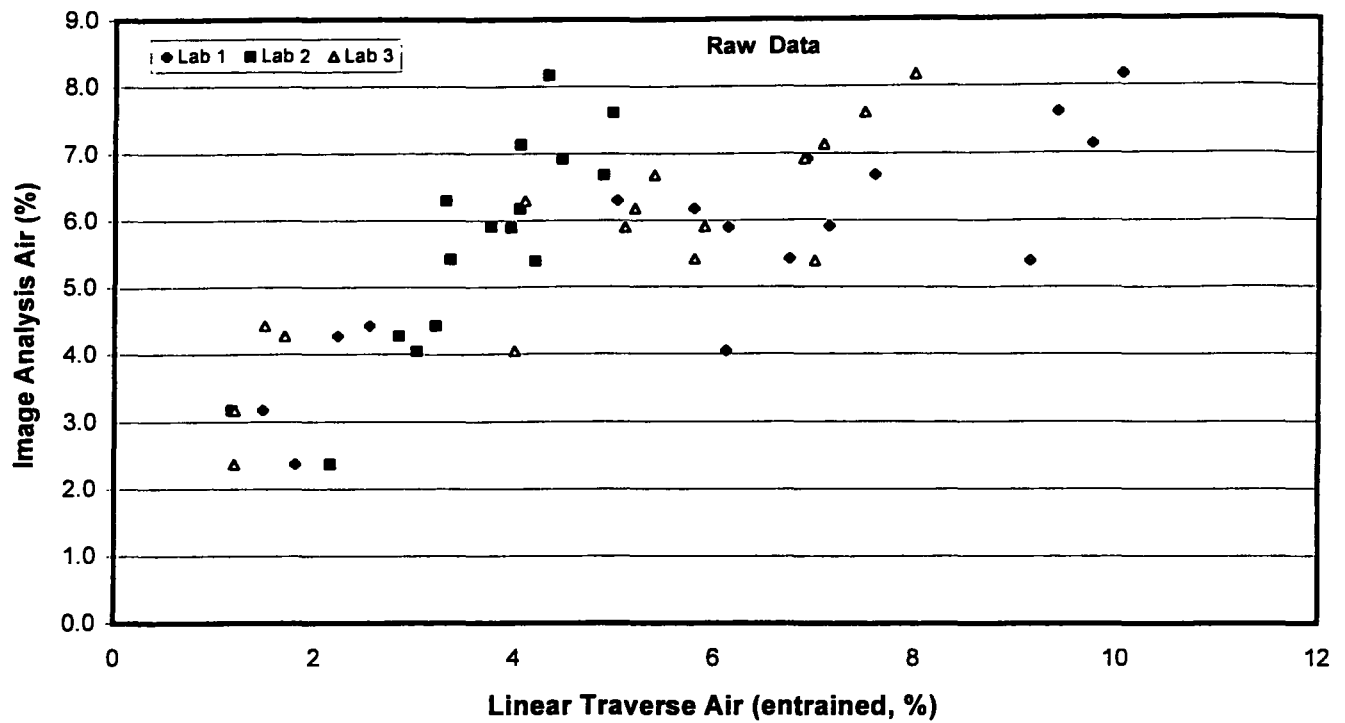
Figure 14. Comparison of image analysis and linear traverse results. Tests were conducted on specimens that were prepared at each lab.
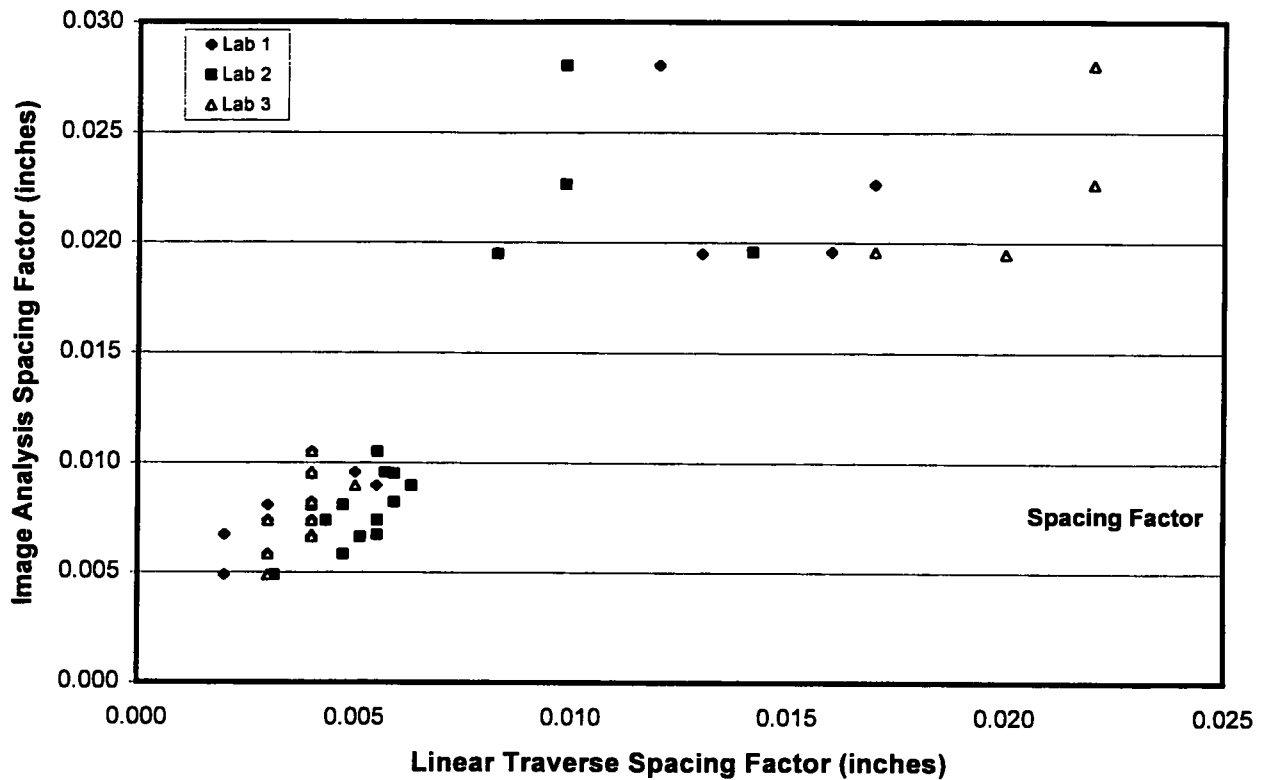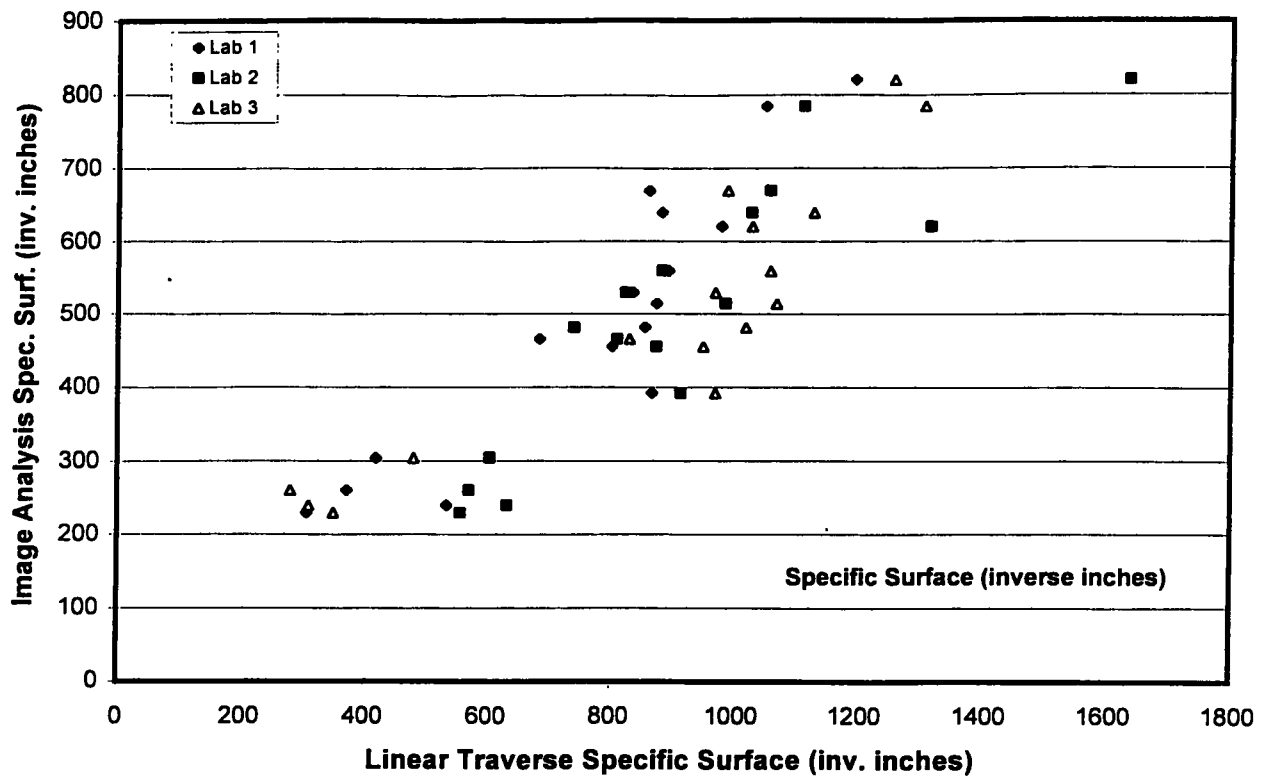
Figure 15. Comparison of specific surface and spacing factor for the linear traverse and image analysis tests. Samples were prepared at each lab with their own procedure.

than a small void (refer to Figure 2 for an illustration of this fact). Hence, the test results that will be reported in this section of the report have been expressed in a "raw data" format. No attempt has been made to correct the void size distribution curves for the probability of observing the specific features. This reconstruction of the void volume (or bubble size distribution, which is a three-dimensional construct) can be done as described in reference 3, however, it was considered to be outside the scope of this research project.

The linear traverse test can produce information describing the void size distribution if the analyst records the chord length for each individual void observed during the traverse. Typical results obtained and reported by the three labs used in this study are shown in Figure 16. The three labs reported rather different chord length distributions for the sample shown in Figure 16, this was the case for most of the samples that were analyzed. This particular sample was chosen for comparison because it contained approximately 6% air, which should have given an adequate number of voids to produce reliable distribution curves. The test results from lab 2 appear to be different from the remaining two labs because it counted a much higher number of very small voids. Also, the chord size distribution that was reported by lab 1 approached zero at a chord length of about 25 microns. The other two labs indicated that they could each still count approximately 500 features with a chord length of 25 microns. It was not apparent which of the three labs produced the most accurate representation of the actual chord-size distribution curve.

The results calculated from the image analysis tests are shown in Figure 17. Note, that the results were calculated from the void area measurements by assuming that each void had a circular shape. The results of similar calculations conducted on other samples, with air contents from about 3% through 9%, have also been plotted on Figure 17. The void-diameter distributions all exhibited nearly the same shape but the number of features that were counted varied considerably. The specimens that had low air contents (and poor freeze-thaw durability) tended to be deficient in voids with diameters ranging from about 10 to 300 microns.

Another way of viewing the image analysis data is shown in Figure 18. This figure presents the raw data (area measurements) obtained from the image analysis procedure. The information has been plotted on an absolute scale so that differences in air content are readily evident on the figure. The
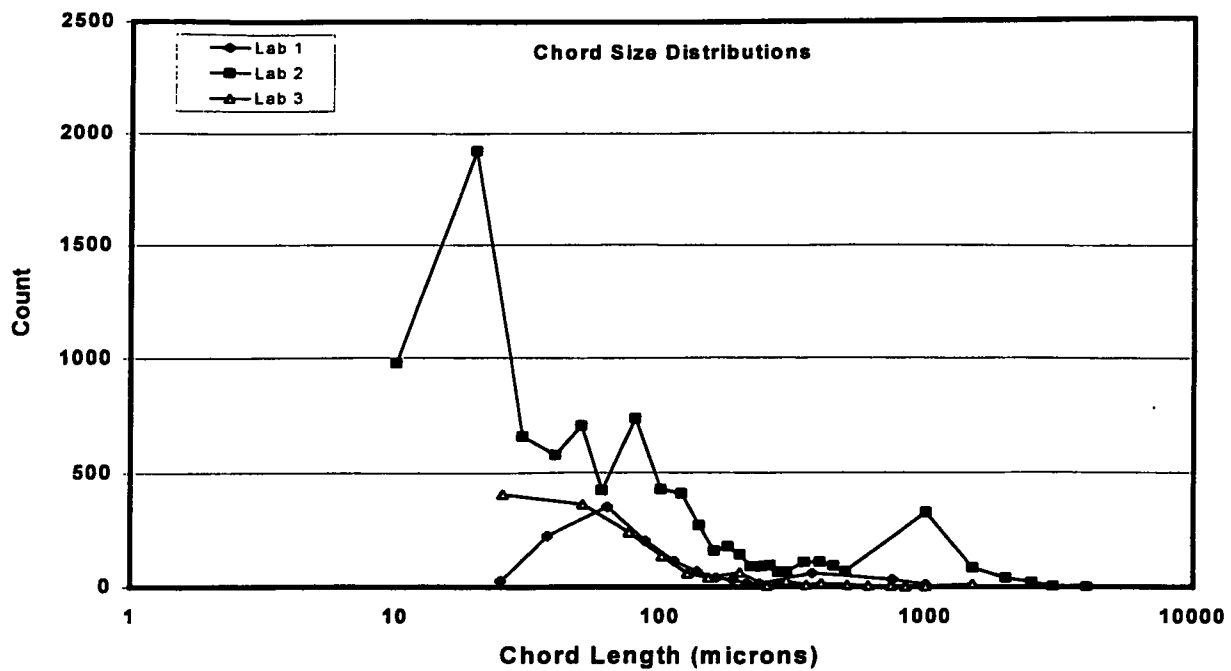
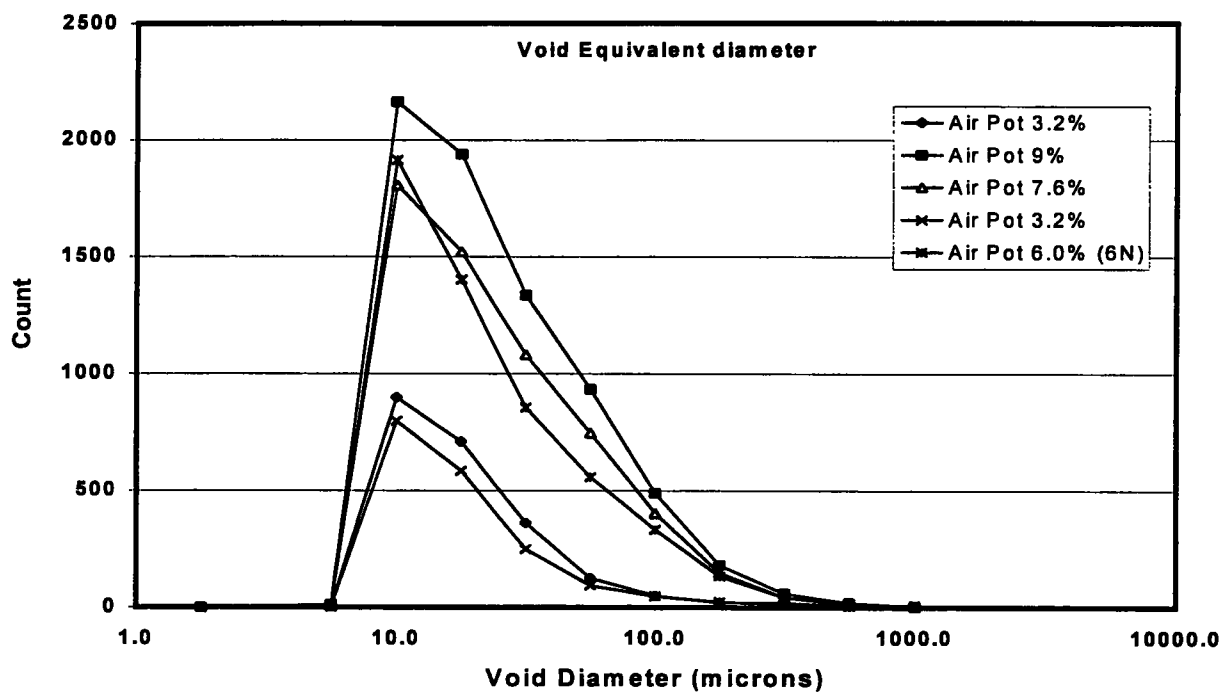Figure 16. Chord length distributions from the linear traverse tests, sample 6N.

Figure 17. Void-diameter distributions from the image analysis tests (various samples).
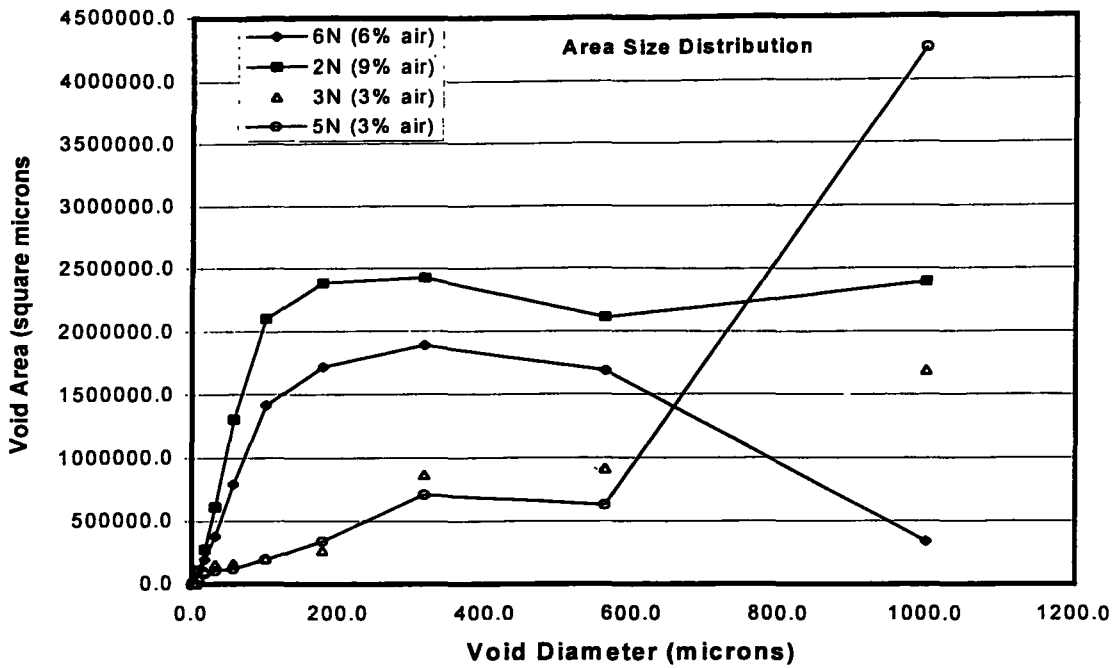
Figure 18.   Void area distributions from the image analysis tests (various samples).
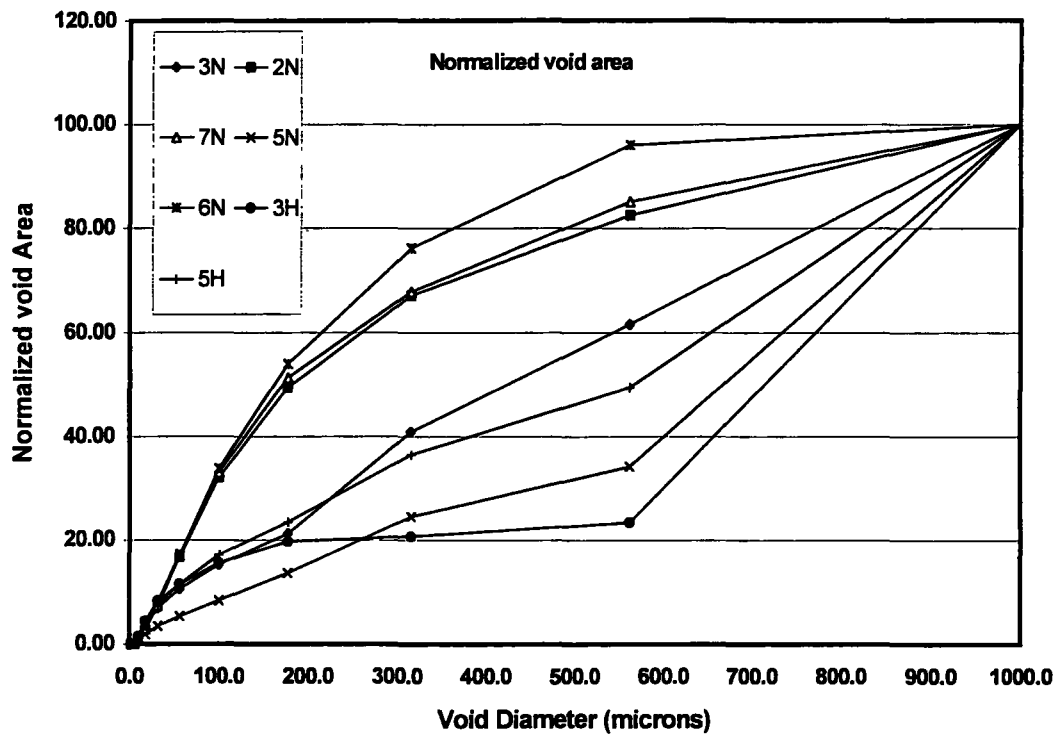

Figure 19.   Normalized void-area distributions from the image analysis tests (various samples).

raw test results can be normalized as shown in Figure 19, or reported on a cumulative basis as shown in Figure 20. In each instance it was is very easy to identify the test specimens that exhibited poor resistance to freezing and thawing – they tended to produce few air voids less than 300 microns in diameter and they often contained an excess of voids larger than 500 microns. Often, 50% or more of the total air content consisted of voids larger than 500 microns (see Fig. 19). In contrast, the durable concrete specimens always exhibited a large amount of small air voids (approximately 70% were smaller than 300 microns in diameter). Each of the three graphs has strengths and weaknesses. The last graph (Fig. 20, the cumulative void area curve) is probably the most useful of the different representations because it provides an absolute indication of the air content of the sample plus it gives an indication of the distribution of void area throughout the different void size classes.
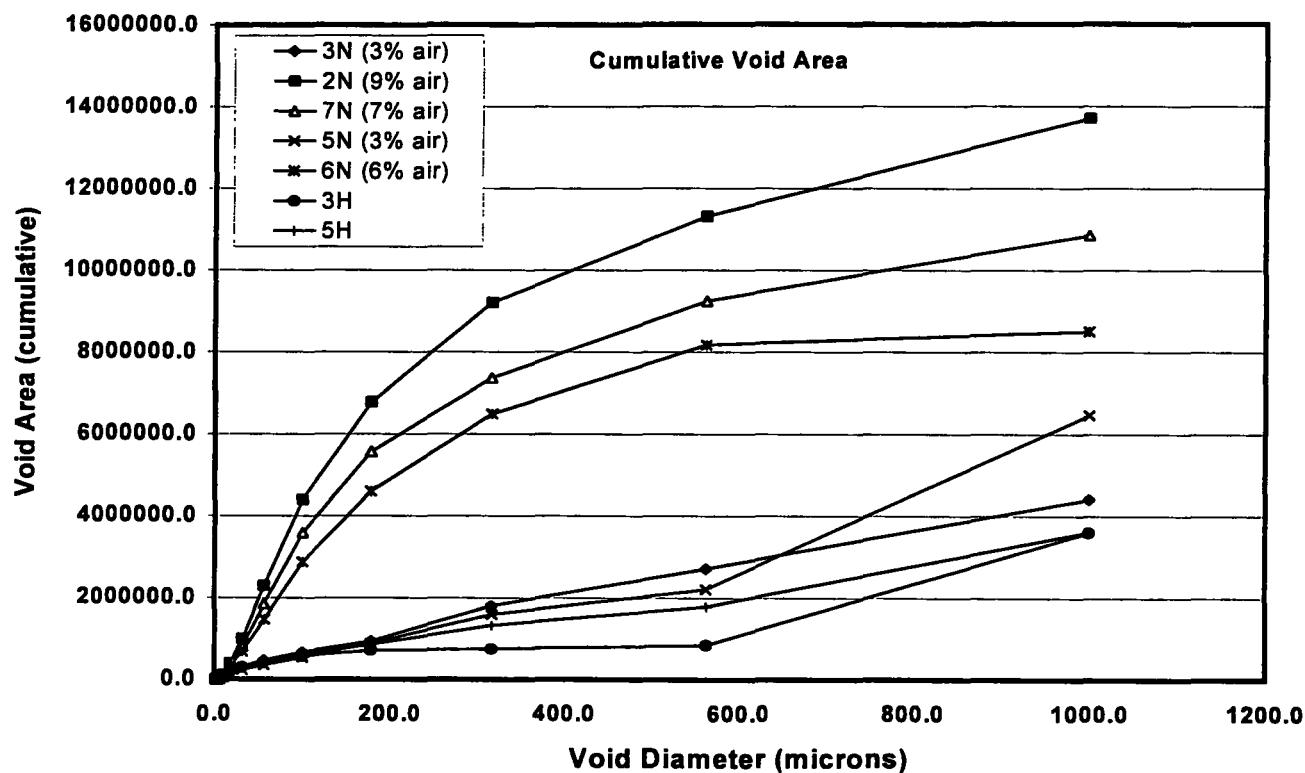
Figure 20. Image analysis void-size distribution curve (cumulative basis).

38

Does the image analysis technique provide a better indicator of the frost-prone concrete than the linear traverse test? This question is hard to answer succinctly. The information presented earlier indicated that both techniques clearly identified the test specimens that exhibited poor resistance to freezing and thawing. Or did they? A graph of linear expansion versus the number of freeze-thaw cycles for the four specimens that were frost prone is shown in Figure 21. Test results for two durable test specimens have also been plotted on the figure. The details pertinent to these particular test specimens have been summarized earlier in this report; however, for the sake of convenience they are repeated again in Table 16. The values reported in the table have been averaged using the data obtained from the various labs. The vibration treatment appeared to have played an important role in the failure process – all of the test specimens subjected to the high vibration treatment exhibited larger slopes in the freeze-thaw tests than the specimens that were subjected to the normal vibration treatment (see Figure 21 or the last column of Table 16; note that the effect was negligible in the specimens containing 6% air). The air content determinations (both linear traverse and image analysis estimates have been averaged together) indicated that the high vibration treatment should decrease the durability because the air content decreased. However, the other two properties reported in Table 16, namely specific surface and spacing factor (only the linear traverse results have been included in the average), contradicted this observation. Specific surface increased and spacing factor remained nearly unchanged. These observations are in agreement with other studies that have reported similar trends [20, 21, 22, 23]. In fact, the data from Table 16 roughly corresponds to the data presented by other researchers [21] (see Figure 22). Note, that the mix proportions summarized in reference 21 were different from those that were used in this study and that the water-cement ratio was considerably lower in this study (nominally 0.4 versus 0.5). However, the fact remains that the vibration treatment lowered the durability of the test specimens but the global properties that are commonly used to assess the relative durability of the different concrete specimens are not sensitive to such treatments.

The same can be said about the image analysis test results. The cumulative void area curve (see Figure 20) clearly indicates that the vibration treatment reduced the magnitude of the void area curves in the size
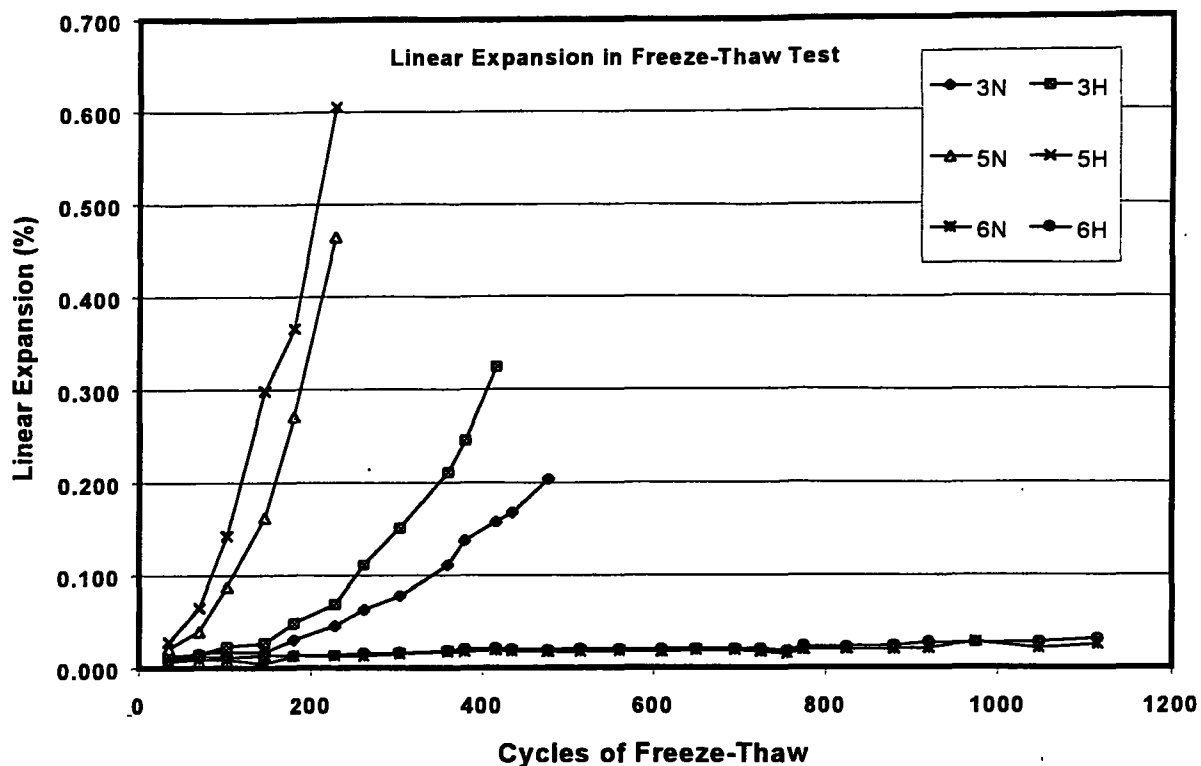
Figure 21. Linear expansion versus cycles of freezing and thawing for several test specimens. Note how vibration influences the results.

Table 16. Average values for a selected series of test specimens.

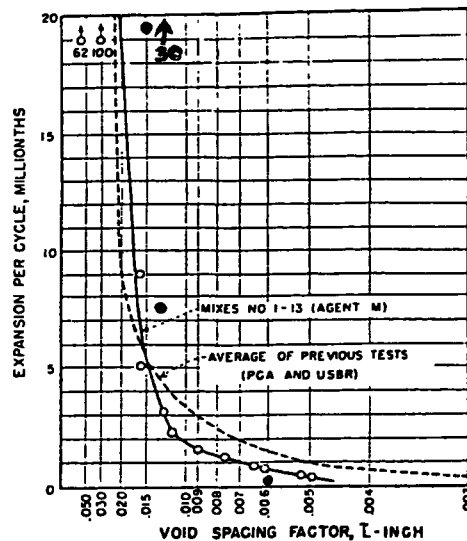| Specimen	Vibration	Air Pot (air, %)	Hardened Air (avg. %, entrained)	Specific surface (avg.,in.$^{-1}$)	Spacing factor (avg., in.)	Freeze-thaw curve slope (millionths)
3	N	3.2	2.6	345	0.014	7.4
3	H	-	1.5	540	0.013	13.2
5	N	3.2	2.8	340	0.015	30.4
5	H.	-	1.6	540	0.014	36.0
6	N	6	4.9	800	0.006	0.2
6	H	-	4.7	890	0.005	0.3

Figure 22.   Relationship between linear expansion during freezing and
thawing and spacing factor (graph from reference 22).

range from about 200 to 600 microns. This would lead one to predict that the
specimens subjected to the high vibration treatment should perform worse
than the other specimens in the freeze-thaw tests (as was observed).
However, the image analysis test results still were not totally consistent with
the failure trend indicated by the durability tests (i.e., order of decreasing
durability as follows: 3N, 3H, 5N and 5H). Perhaps looking at feature specific
information (i.e., frame by frame estimates) would help to place the image
analysis measurements in better agreement with the distress that was
observed.   This would be an excellent area to concentrate on in future
research programs. An example of how this can be done is shown in Figure
23. This figure uses a bar chart to illustrate the image-by-image air content
for sample 5.   The air contents are expressed on a mortar basis (not a
concrete basis) so an air content of about 9% to 10% would be considered
"normal" for a properly air-entrained specimen. The top half of the figure
shows the individual air contents after the normal vibration treatment. The
bottom half of the figure shows the individual air contents after the high
vibration treatment. It is very clear that the vibration treatment decreased the
air content below the 2% level in many of the images that were collected. This
extra flexibility of the image analysis method is useful because freeze-thaw
cracking apparently starts in specific regions (i.e., it is a feature specific event,
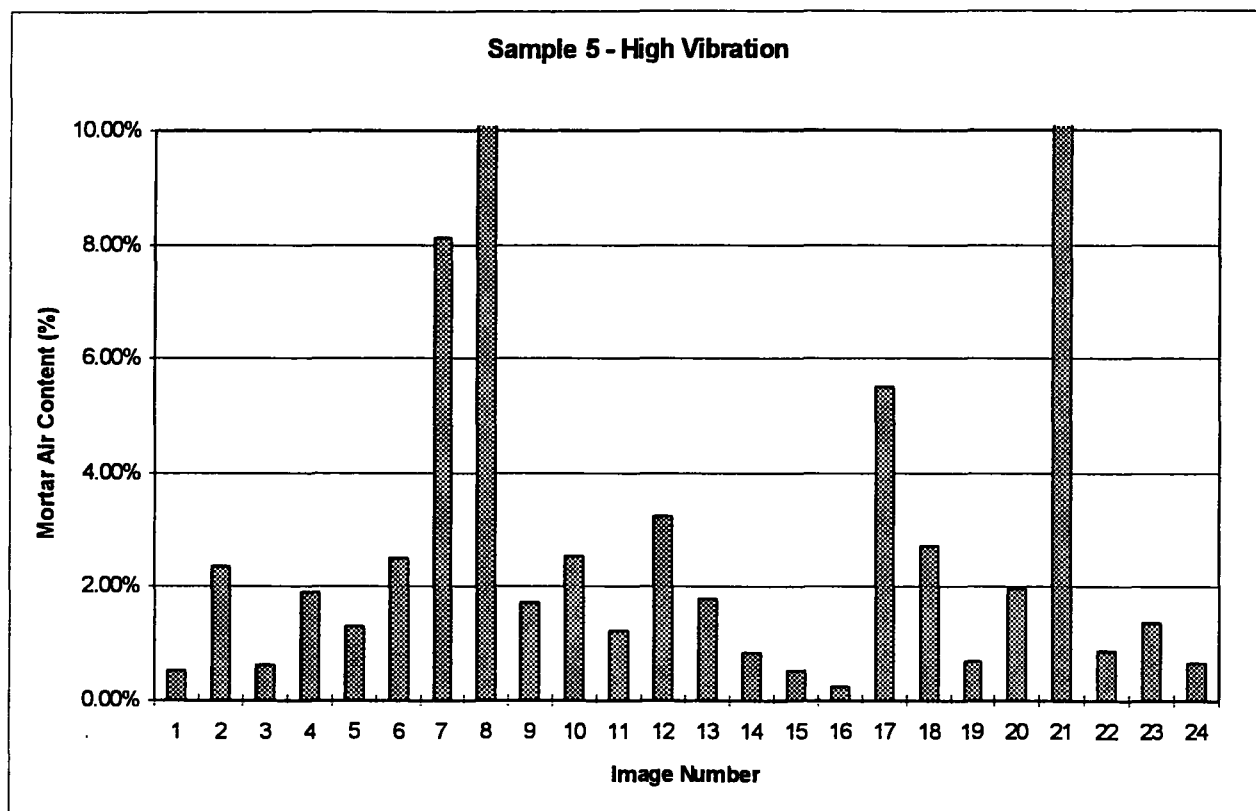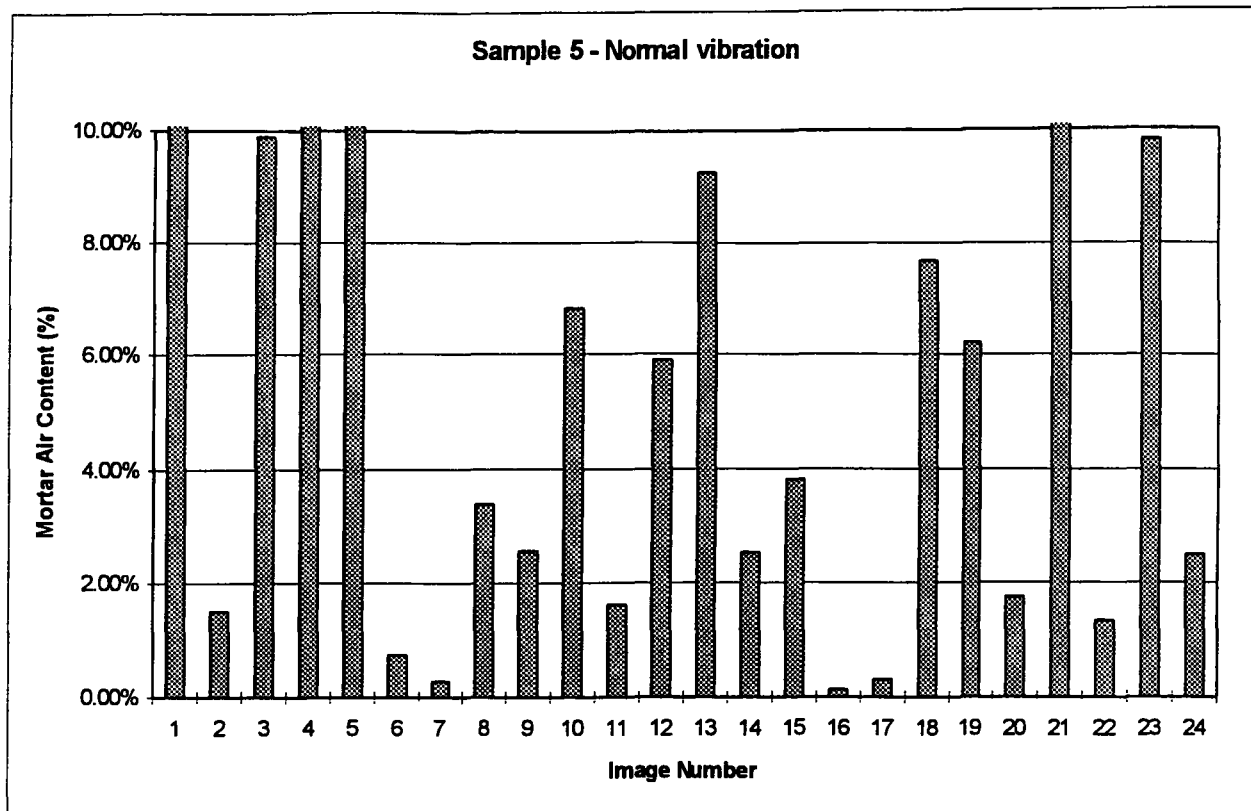rather than a global event) that are inadequately protected by the air-voids.

41

Figure 23.   Image-by-image air contents for the specimens from concrete
mix 5. Note how vibration often reduces the air content below 1%.

SUMMARY AND CONCLUSIONS

In summary, this project has investigated the use of image analysis to measure the air content and distribution of the entrained-air void system in portland cement concrete. The study evaluated these properties in a series of eight concrete mixes that were made and cured under standard laboratory conditions. The air contents of the various mixes ranged from about 3 to 9 percent. Four of the mixes contained 20% fly ash, which was substituted for portland cement on an equivalent mass basis. The study also included different vibration treatments that were used in an attempt to distort the entrained-air void system.

The results of this research effort, which was directed at creating a routine procedure for analyzing the entrained-air void system in portland cement concrete, can be summarized as follows:

1. The routine procedure that was developed and detailed in this study can be used to give reasonable estimates of the entrained-air content of laboratory concrete specimens. The test results indicate that the values are in good agreement with those that were determined using the standard testing procedure for hardened concrete (ASTM C 457). It currently takes approximately one hour per specimen to conduct the image analysis test for entrained-air content.

2. The calculation of specific surface and spacing factor from the image analysis process are different from those calculated from the linear traverse test. This was due to the area weighting that was used to stabilize the mean void diameter from the image analysis tests. This is of little concern since the image analysis test results were still able to separate durable concretes from those that were prone to freeze-thaw attack (as measured by ASTM C 666, method B).

3. The vibration treatments that were used in this study did not adequately distort the entrained-air void system of the concrete specimens. This was in contrast with field studies that have implicated excessive vibration as a major contributor to destruction or distortion of the entrained-air void system. This lack of agreement between field and lab observations is most probably due to the fact that the mixing cycle in laboratory concrete is so long that

43

it tends to form a better distribution of the entrained-air voids. The laboratory test results clearly indicate that the smaller entrained-air voids are difficult to vibrate out of the specimens. Typically, one would expect that the larger voids, or those that have coalesced due to inadequate mixing and dispersion, are much more prone to being vibrated out of the concrete.

4. The Air Void Analyzer test was not used enough to form any significant conclusions pertaining to the concrete mixes that were studied in this project.

5. The high-pressure air method for determining the hardened air content of the concrete test specimens exhibited excellent correlation to the plastic air content of the various mixes. In most instances it was able to provide a very accurate estimate (±0.5% absolute) of the original air content. It is not known if this excellent agreement would be obtained from field specimens of concrete because of the potential for filling entrained-air voids with recrystallized minerals.

6. Fly ash appeared to have little influence on the air content or air-void distribution of the test specimens that were made in this study.

RECOMMENDATIONS

This study has indicated that image analysis can play an important role in the measurement of entrained-air void systems and the documentation of the information pertaining to the fundamental constituents that are normally observed in portland cement concrete. These are areas that have historically been dominated by conventional light microscopy and practicing petrographers. However, the application of scanning electron microscopy to this area has tremendous potential. This potential is based in part on the tremendous resolution and easy access to elemental information that are commonly available on an SEM, but it also hinges on the high level of documentation and subsequent analysis that come from digital imaging techniques. Hence, it is recommended that efforts should be directed at:

1. Verifying the correlations observed in this study, between linear traverse and image analysis tests, with independent testing of field concrete specimens. This really needs to be done before the technique can be adopted on a routine basis. Previous research [11] has noted significant differences between laboratory and field

44

concrete specimens. Also, this study was limited to laboratory testing using rapid freezing and thawing to estimate durability, this test procedure has exhibited only poor correlation to Iowa DOT field service records. Hence, verification of the features that will be used to denote "good" and "bad" air void systems is strongly recommended.

2. Further work should be conducted to investigate the use of image analysis to estimate the water/cement ratio, measure the paste content and to count the particles of unhydrated cement in concrete.

ACKNOWLEDGEMENTS

REFERENCES

1. High Performance Construction Materials and Systems- An Essential Program for America and its Infrastructure, Executive Report, Report 93-5011.E, April, 1993.

2. American Society for Testing and Materials, <u>1997 Annual Book of ASTM Standards</u>, Vol. 4.02, ASTM, West Conshohocken, PA, 1997.

3. Russ, J.C., Computer-Assisted Microscopy The Measurement and Analysis of Images, Plenum Press, New York, 1990.

4. Larson, T.D., P.D. Cody and J.J. Malloy, "The Protected Paste Volume Concept Using New Air-Void Measurement and Distribution Techniques," Journal of Materials, Vol. 2, No. 2, March 1967, p. 202.

5. Chatterji, S. and H. Gudmundsson, "Characterization of Entrained Air Bubble System in Concrete by Means of an Image Analyzing Microscope," Cement and Concrete Research, Vol. 7, No. 4, 1977, p. 423.

6. Roberts, L.R. and P. Scheiner, "Microprocessor-Based Linear Traverse Apparatus for Air-Void Distribution Analysis," in the Proceedings of the Third Int. Conf. On Cement Microscopy, G.R. Gouda editor, International Cement Microscopy Assoc., Duncanville, TX, 1981.

7. Laurencot, J.L., R. Pleau and M. Pigeon, "The Microscopical Determination of Air Voids Characteristics in Hardened Concrete: Development of an Automatic System Using Image Analysis Techniques Applied to Micro-Computers," in the Proceedings of the Fourteenth Int. Conf. On Cement Microscopy, G.R. Gouda, A. Nisperos and J. Bayless editors, International Cement Microscopy Assoc., Duncanville, TX, 1992.

8. Oren, G., F. Manwiller and K. Bergeson, Image Analysis for the Characterization of Materials for Highway Construction, Iowa DOT Project HR-346, Phase I Progress Report, Nov. 30, 1992.

9. Oren, G. V. Marks and W. Dubberke, "Image Analysis of PCC and ACC Pavements Using SEM Images", Transportation Research Record 1458, 1994.

10. Air Content by Image Analysis of 4" by 9" PCCP Cores, J. Grove, G. Oren and W. Dubberke, a study dated Oct. 29, 1993. Internal report.

11. Schlorholtz, S. and J. Amenson, Evaluation of Microcracking and Chemical Deterioration in Concrete Pavements, Iowa DOT Report HR-358, Final Report, Oct. 31, 1995.

12. Significance of Tests and Properties of Concrete and Concrete Making Materials, ASTM STP 169B published 1978, and ASTM STP 169C published 1994, by ASTM, Philadelphia, PA.

13. Magura, D., Air Void Analyzer Evaluation, Federal Highway Administration Report No. FHWA-SA-96-062, May 1996.

14. Magura, D., "Evaluation of the Air Void Analyzer," Concrete International, August, 1996.

15. LINK ISIS Operators Manual, MANREV3.0, OXFORD Instruments Microanalysis Group, UK, 1995.

16. American Society for Testing and Materials, <u>1997 Annual Book of ASTM Standards</u>, Vol. 4.01, ASTM, West Conshohocken, PA, 1997.

17. Sommer, H., "The Precision of the Microscopical Determination of the Air-Void System in Concrete," Cement, Concrete, and Aggregates, Vol. 2, No. 1, 1979, p. 49.

18. Pleau, R., P. Plante, R. Gagne and M. Pigeon, "Practical Considerations Pertaining to the Microscopical Determination of Air Void Characteristics of Hardened Concrete (ASTM C 457 Standard)," Cement, Concrete, and Aggregates, Vol. 12, No. 2, 1990, p. 3.

19. Walker, H.N., "Formula for Calculating Spacing Factor for Entrained Air Voids," Cement, Concrete, and Aggregates, Vol. 2, No. 2, 1980, p. 63.

20. Mielenz, R.C., V.E. Wolkodoff, J.E. Backstrom and H.L. Flack, "Origin, Evolution, and Effects of the Air Void System in Concrete. Part 1- Entrained Air in Unhardened Concrete," Proceedings, American Concrete Institute, Vol. 55, 1958, p. 95.

21. Backstrom, J.E., R.H. Burrows, R.C. Mielenz, and V.E. Wolkodoff, "Origin, Evolution, and Effects of the Air Void System in Concrete. Part 2- Influence of Type and Amount of Air-Entraining Agent," Proceedings, American Concrete Institute, Vol. 55, 1958, p. 261.

22. Backstrom, J.E., R.H. Burrows, R.C. Mielenz, and V.E. Wolkodoff, "Origin, Evolution, and Effects of the Air Void System in Concrete. Part 3- Influence of Water-Cement Ratio and Compaction," Proceedings, American Concrete Institute, Vol. 55, 1958, p. 359.

23. Mielenz, R.C., V.E. Wolkodoff, J.E. Backstrom and R.H. Burrows, "Origin, Evolution, and Effects of the Air Void System in Concrete. Part 4- The Air Void System and Job Concrete," Proceedings, American Concrete Institute, Vol. 55, 1958, p. 507.

Appendix I

(Standard Operating Procedure for Image Collection and Analysis)

Standard Operating Procedure for Image Analysis of Concrete

The purpose of this document is to summarize the steps that are necessary to prepare, measure and analyze portland cement concrete cores using image analysis. This documents only the rudimentary steps that need to be performed, some studies may benefit considerably from the use of additional steps, such as filtering or contrast enhancement.

Sample Preparation

Sample preparation is a critical step in this technique. The purpose of this step is create a flat surface that can be ground and polished to reveal surface details such as air voids, aggregates and cement paste. If the specimen cannot be made flat in a reasonable amount of time using the grinding paper listed in step 1, then a coarser paper (say 100 or 120 grit) can be used. However, it is important to understand that step 1 must produce a flat specimen because there is no point in performing steps 2 through 5 if the sample has not been ground to a flat surface. Excessive surface pressure during the early grinding steps can destroy the sample surface, especially when the concrete is soft or micro-cracked. As always, practice and experience play a key role in producing specimens with a high-quality surface.

Briefly, the method consists of: (1) sawing off a section of the concrete core (diamond blade, propylene glycol used as a coolant); (2) rinse off the propylene glycol using tap water; (3) grinding the sample surface flat by using fixed grit paper and the 12 inch grinding/polishing wheel described earlier in this report (grit sizes listed in Table A1, water used as a lubricant). This sample preparation method is very similar to the method that is commonly used to prepare specimens for air void analysis by standard ASTM procedures [2].

Table A1.   Grinding and polishing procedure for the concrete cores.

Step	This method grit size (micron equiv.)	ASTM C 457 (see [6]) grit size (micron equiv.)
1	180 (70μm)	100 (150μm) optional
2	320 (30μm)	220 (75μm)
3	600 (17μm)	320 (35μm)
4	800 (12μm)	600 (17.5μm)
5 (optional)	1200 (2 to 5μm)	800 (12.5μm)

Data Collection

Data collection will normally be accomplished using the Hitachi 2460N (low-vacuum) scanning electron microscope. However, as access to better stage controllers improves and contrast enhancement procedures are refined, data could also be collected using any type of instrument that produces high-quality (1024 x 768 resolution) digital images. This section summarizes the normal steps that need to be followed to collect data using the Hitachi SEM.

1. Turn on the Helium gas and connect it to the SEM.
2. Vent the SEM chamber (AIR/EVAC button) so that you can insert a specimen. Check to make sure that the sample stage is at its default position (X=60, Y=25). If it is not in the default position then position it there manually or by pressing CAL, 9, ENTER on the DEBEN stage control panel.
3. Turn on the SEM using the right breaker located on the base of the SEM column. This will energize the viewing CRT.
4. Turn on the infrared camera to view the contents of the SEM chamber.
5. Slide the Robinson detector out of the SEM chamber.
6. Wind the LINK X-ray detector up to get it out of the way.
7. Slide the LINK TETRA detector into the SEM chamber.
8. Place the specimen to analyzed on the circular or square specimen holder (make sure that the surface of the sample is level with the edges of the sample holder) and then attach the reference standard to it. The reference standard can be placed on any coarse aggregate particle near the center of the specimen. It is best to position the reference standard with the white side to the 12:00 position. This assumes that the raster rotation is not on!
9. Slide the sample into the SEM chamber and press the AIR/EVAC button to pump the chamber down. Set the pressure level at 40 Pa using the F2 key.
10. Set the image selector (SE-Xray-AUX) switch to AUX
11. Turn off the infrared camera.
12. Set the PCI-TETRA slide switch to TETRA.
13. Set the accelerating voltage to 6.0 kV.
14. Set the beam current to 240 using the F10 key.
15. Set the working distance to 11 mm.
16. Turn on the accelerating voltage.
17. Log in to the ISIS software package and start the TETRA, AUTOBEAM and AUTOANALYSIS software packages. Arrange the various windows on the screen in a position that you feel comfortable with.
18. Select the TETRA window and recall the test conditions for the "6kV, new Tetra" setup. The display CRT should show an image of the specimen surface. Focus the image using the Hitachi controls and a moderate level of magnification (say 200 or 300x). Decrease the magnification to the

working level (40x in most instances or 50x for very small features) and refocus if necessary.

19. Locate the reference standard on the specimen surface and center the white-black region of the image on the viewing CRT. Depress the static line profile mode button. Tweak the TETRA using the software controls to set the low and high levels of contrast and brightness to the green lines drawn on the photo CRT.

20. Check for level illumination by moving the reference sample to show a totally black image and then depressing the static line profile mode button. A flat horizontal line should be observed. Tweak the SEM gun controls as needed to level the line.

21. Select the AUTOANALYSIS window and start a new AUTOANALYSIS run. Select the areas to be imaged by using the DEBEN stage control to position the stage at the various stop points and then press the left-mouse button to store that location in the AUTOANALYSIS measurement queue. Repeat this procedure until 20 points have been selected. Then initiate the AUTOANALYSIS run. Each run consumes over 20 MB of hard disk space so plan accordingly.

Procedure for Air Void Image Analysis
Notes, Caveats, and Warnings

Menus - ImQuant does not strictly follow Windows menu conventions. Shortcut keys are not always underlined. Often it is necessary to select a letter twice if using keyboard shortcuts, e.g., Analyze Individual (it comes after Interactive).

Display mode - The display should be set to 256-colors mode with a resolution of either 1280x1024 or 1600x1200. QuickRes on the TaskBar allows quick changes between modes. (Using 256-color mode will increase the speed of response and is needed to allow the graphics toolbox to work properly. Higher resolutions allow for less overlap of the necessary windows.)

File location - Data should be copied from the Link to a local hard disk for speed of processing. The files common to the Isis dataset and job must be copied in their entirety, but data files may be copied in part, as needed. Use ImQuant or AUTOBEAM to determine which files to copy.

64 file limit – Oxford's code for reading ISIS files into Visilog has a bug that only allows reading about 64 files per session before running out of memory. That is equivalent to about 2-1/2 batches of 24 images. You exit Visilog completely and restart it to restore the memory

1. Startup

Set video mode	QuickRes on Taskbar
Start recorder macro set	Run C:\WIN\EXCELR.REC and minimize.
Start Isis Labbook	
Select job	

Start ImQuant	
Load AIR.J into C Interpreter	File-Load
Declare the macro	position cursor in routine name then select Interpreter-Declare
Close Interpreter	
Bring up current commands window (in IMQuant)	Display-Current Commands
Prepare Analysis	(in IMQuant) Analyze-Individual Specify images: label for Label image, raw for Grey image, filter for Filter image (this is case sensitive!) Select measures to analyze (Surface, Perimeter, Shape)
Record internal names of files	It is easier to edit the DOS file name in the Read dialog than to use the Disk icon to select files. DOS file names can be found via the Disk icon or in AUTOBEAM.
Read first image into 'raw'	File-Read then click Disk icon
Set spatial calibration	Analyze-Calibration-ISIS Calibration
Check calibration values	(in Command Panel) type printf(SCALE_X) <RET>, and printf(SCALE_Y) <RET> Values should be close to 2.41 for 50x images with 1024 pixels. Perform manual calibration if necessary.
Optional manual calibration	This requires separate X and Y calibrations under Analyze-Calibration. The image is 2473x1932 microns at 50x. Those values may be used for the X and Y distances and the scale bar extended to reach the sides of the image. Press the right mouse button and choose Exit to save the calibration. Recheck as above.
Store macro name in paste buffer	Select Command Panel center window Type AIR() and copy it to paste buffer (Select the text with Shift-Home, cut with Shift-Delete, paste back in with Shift-Insert)

2. Processing Images

Start macro sequence	Paste AIR() back into Command Panel (Shift-Insert), Press Enter
Edit the file name	6 spaces left, Backspace, Enter new index

Review/Set thresholds	Lower threshold should be set to zero Upper threshold should be set as high as possible to include the maximum porosity without selecting excessive pixels of aggregate or paste. **THIS STEP IS CRITICAL!** Some pores will be missed, some aggregate porosity will be included, and some small, dark regions of aggregate may be included. These effects will offset each other some, but be careful.
Select Analysis	Wait for Label operation to finish, then press Alt-Tab twice (more or less if out of sequence)
Update series name	e.g., A4-T13 (Pressing return after editing the label is intuitive but won't help or hurt anything.)

(The following few steps are defined as a macro with Ctrl-Alt-Z as the hot key.)

Analyze frame	Analyze-Go Wait for analysis to finish; the area dialog in IMQuant will change.
Examine results	Particles larger than 785K sq. um have an equivalent diameter larger than 1000 um and will fall outside the size tables and require corrective steps. Large, contacting particles may be separated using Graphics Toolbox. Particles with an area of 5.83 sq. um contain only a single pixel at 50x. They should not exist following processing.
Ship to Excel	Alt-I-E (Display Excel
Switch to Command Panel	Wait for "display to Excel" to finish; the first time takes awhile. Press Alt-Tab twice (more or less)

Repeat this process until all 20 frames have been analyzed

3. Combining Results

A Windows macro has been defined to aid in this process. It should be automatically loaded when Windows starts. If not loaded, open EXCELR.REC in the Windows directory before proceeding. Some tweaking of the timing may be needed depending on the computer and configuration. (Note: Excel-95 performs much better than Excel–97.)

Switch to Excel Window	
Open TEMPL-20 spreadsheet	Cursor should be positioned in the first particle index cell (i.e., B12). This must be

	spreadsheet window number 1 for the macro to work - it will be if opened last.
Activate first result spreadsheet	Shift-Ctrl-Tab, if everything is in order . Check the spreadsheet title for proper number
Activate Macro	Shift-Ctrl-Q The macro will select the data cells and copy the values only to the appropriate location in the template, it will fill in the frame number for all particles in that frame, it will set the next frame number, and it will position the cursor for pasting in the next frame. Therefore, once the sequence is started it should be a simple matter to press the two sequences a total of 24 times. You do not even have to release the Shift and Ctrl keys between the steps - just toggle between Tab and Q.
Clean up the combined spreadsheet	Delete the last frame number entry; it will not be used.
Fill in columns F through J	Start in the lower right cell (J-xx), extend the selection back to column E (Shift-left-arrow), then extend to the top of the particles (End, up-arrow). Press Shift-right-arrow to deselect column E. Press Ctrl-D to fill down Columns F through J.
Update the Pivot Tables	Check that only bins 1 though 10 are used (less is OK, more is bad). Particle records may be sorted based on size and extreme values may be replaced to truncate the size distribution at 785,000 sq.um. Starting with the first table, select a cell in the table and press the update key (! button on the toolbar). Repeat for each of the four tables.
Save the new sheet	Alt-File-SaveAs with an appropriate name.
Print the sheet	Alt-File-Print - Only the summary portion will print.
Close all sheets	Shift-Alt-File-CloseAll
Proceed to next sample	

Appendix II

(Chemistry and mineralogy of the cement and fly ash used in the project)

Table 1, Appendix II. Assays of the cementitious materials used in the mixes.

Constituent (expressed as a oxide)	Portland Cement (LaFarge)	Fly Ash (Port Neal 4)
SiO_2	20.4	35.3
Al_2O_3	4.27	18.1
Fe_2O_3	3.30	5.8
CaO	63.3	26.8
MgO	2.95	4.9
SO_3	2.57	3.2
Loss on Ignition	1.43	0.5
Na_2O	Not Measured	1.3
K_2O	0.75	0.38
TiO_2	0.19	1.42
P_2O_5	0.12	1.16
SrO	0.05	0.41
BaO	Not Measured	0.83

LaFarge cement, Type I, 1/14/97 MEAS0088.MDI

--- LaFarge cement, Type

Port Neal 4 fly ash MEAS0023.MDI
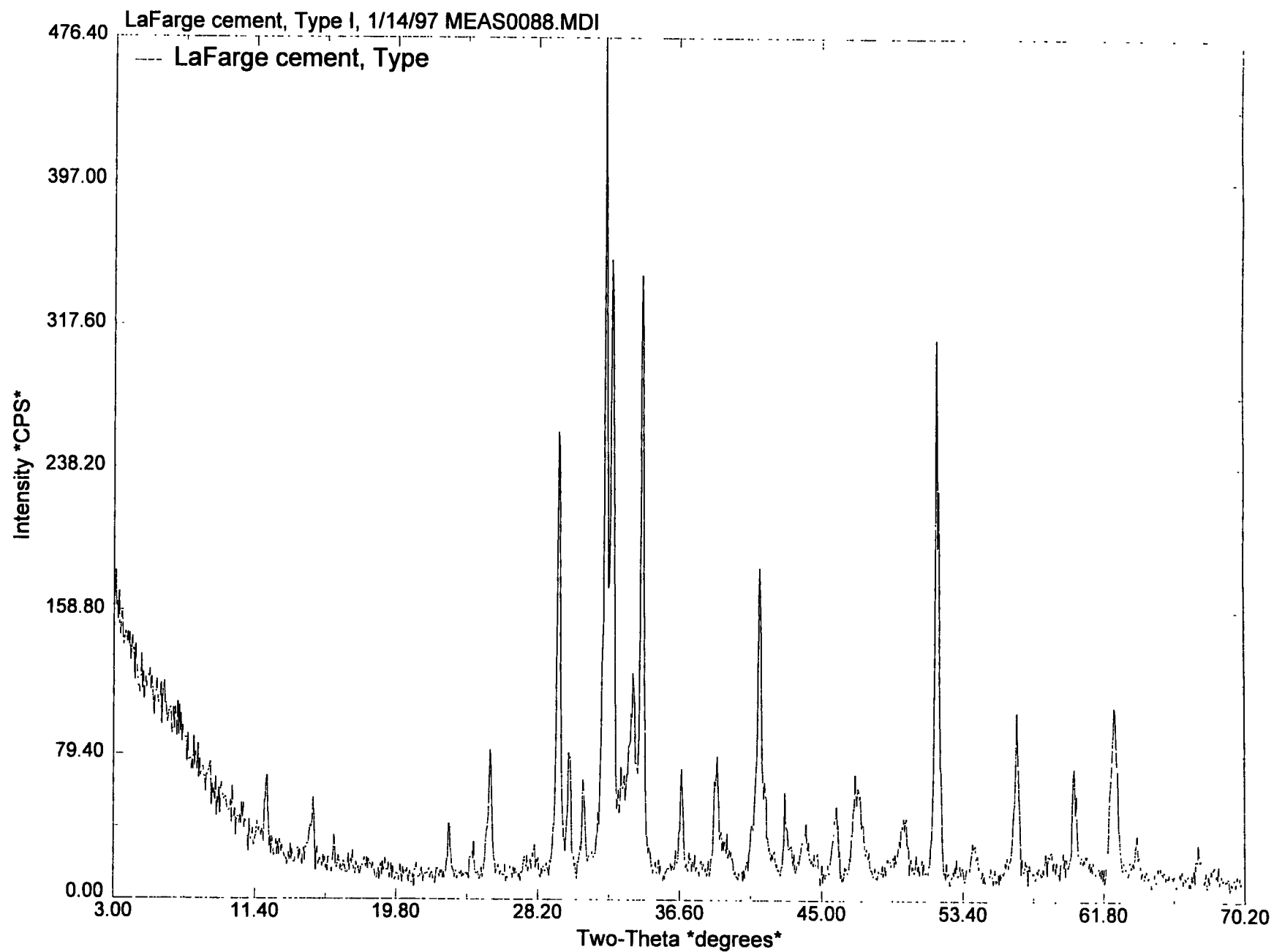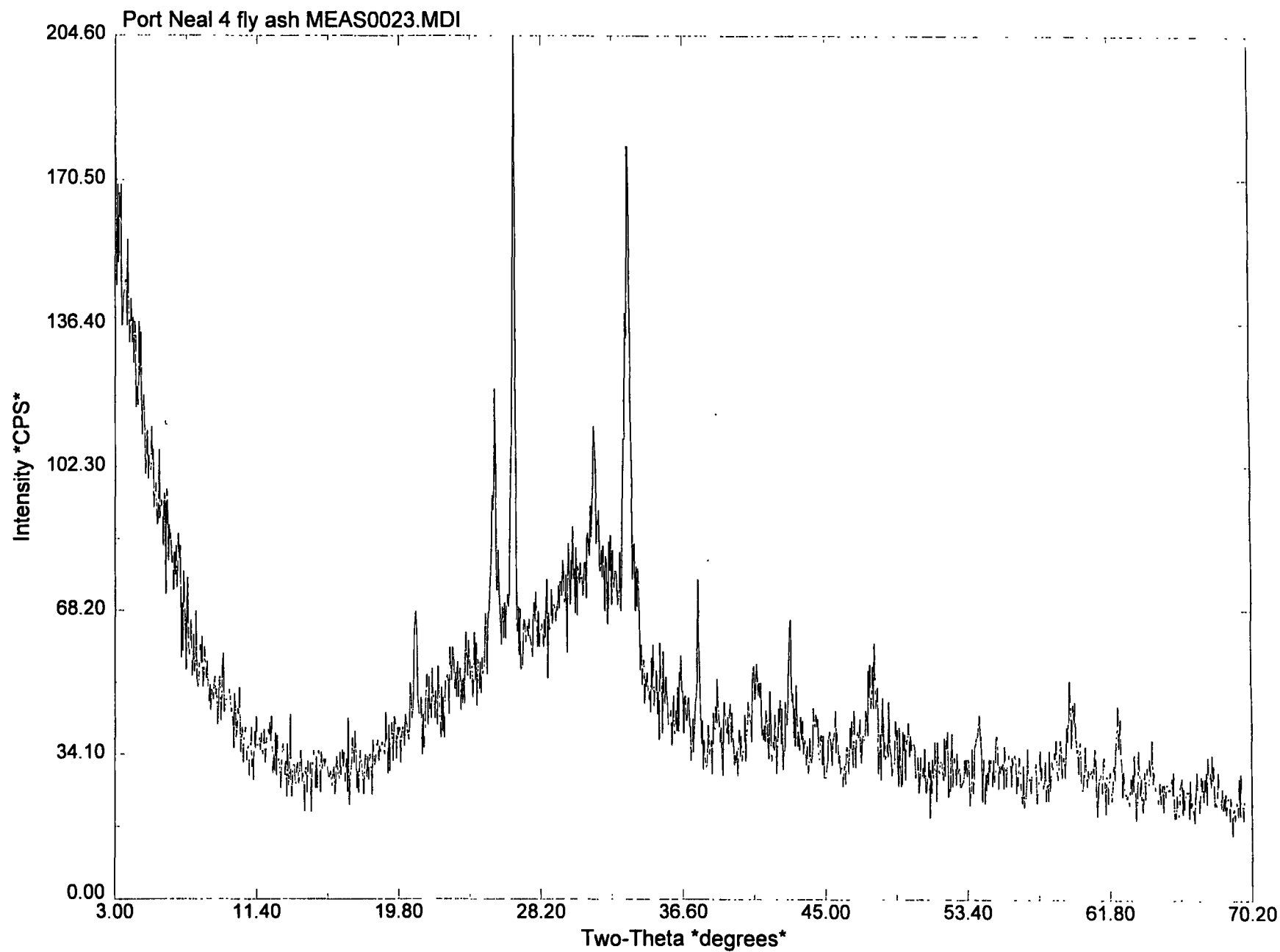
Appendix III

(Typical output from an image analysis test)

Number of divisions/decade	4	
Starting Diameter	3.163	
Bin Factor	1.778	
1 mm bin	10	

	Diam	Bin
Min.	5.45	1
Max.	873.70	10

				Air Void Content	
Mean Diameter	26.42			Mean	12.97%
Diameter-weighted Mean Diam	86.88	Ave(D^2)/Ave(D^1)		Std.Dev.	4.97%
Area-weighted Mean Diam	272.32	Ave(D^3)/Ave(D^2)		Rel.Err.	1.02%

Size Distributions

Eq. Diam

	1.78	5.62	10.00	17.79	31.63	56.25	100.02	177.87	316.30	562.47	1000.23	
Count Fraction BinNum												
Sample	-1	1	2	3	4	5	6	7	8	9	10	Grand Total
(blank)	#DIV/0!	#DIV/0!	#DIV/0!	#DIV/0!	#DIV/0!	#DIV/0!	#DIV/0!	#DIV/0!	#DIV/0!	#DIV/0!	#DIV/0!	#DIV/0!
1	0.0%	0.0%	33.6%	28.9%	12.1%	12.5%	10.0%	1.8%	1.1%	0.0%	0.0%	100.0%
2	0.0%	0.0%	30.9%	26.2%	14.5%	14.5%	7.9%	3.8%	1.9%	0.0%	0.3%	100.0%
3	0.0%	0.0%	30.3%	28.9%	15.9%	15.2%	7.2%	2.2%	0.4%	0.0%	0.0%	100.0%
4	0.0%	0.2%	37.7%	26.5%	14.6%	10.3%	8.3%	0.9%	1.1%	0.4%	0.0%	100.0%
5	0.0%	0.4%	34.7%	28.9%	18.7%	7.7%	6.0%	3.0%	0.4%	0.0%	0.2%	100.0%
6	0.0%	0.0%	32.2%	32.9%	19.7%	6.5%	5.7%	2.0%	1.0%	0.0%	0.0%	100.0%
7	0.0%	0.5%	38.7%	27.3%	17.8%	7.2%	5.0%	2.5%	0.9%	0.0%	0.2%	100.0%
8	0.0%	0.3%	36.6%	30.5%	14.0%	12.2%	3.3%	2.8%	0.0%	0.3%	0.0%	100.0%
9	0.0%	0.9%	40.9%	23.8%	13.2%	10.6%	6.4%	2.6%	1.3%	0.0%	0.4%	100.0%
10	0.0%	0.2%	34.9%	26.7%	15.5%	13.0%	5.7%	2.2%	1.5%	0.2%	0.0%	100.0%
11	0.0%	0.0%	34.5%	23.1%	20.3%	10.4%	7.6%	2.5%	0.9%	0.3%	0.3%	100.0%
12	0.0%	0.0%	30.1%	21.0%	20.3%	14.9%	8.0%	4.0%	1.8%	0.0%	0.0%	100.0%
13	0.0%	0.0%	28.6%	25.8%	20.7%	12.7%	6.6%	3.8%	1.9%	0.0%	0.0%	100.0%
14	0.0%	0.0%	34.4%	28.9%	13.6%	13.8%	7.3%	1.0%	0.8%	0.0%	0.3%	100.0%
15	0.0%	0.0%	31.3%	27.2%	19.0%	12.8%	5.5%	3.1%	0.7%	0.2%	0.0%	100.0%
16	0.0%	0.0%	36.9%	29.0%	12.8%	11.4%	6.6%	2.8%	0.0%	0.7%	0.0%	100.0%
17	0.0%	0.0%	26.9%	31.2%	17.3%	13.5%	8.5%	2.7%	0.0%	0.0%	0.0%	100.0%
18	0.0%	0.0%	24.3%	31.9%	18.7%	12.7%	8.4%	2.0%	1.6%	0.4%	0.0%	100.0%
19	0.0%	0.2%	33.8%	25.3%	17.5%	13.5%	6.9%	1.9%	0.9%	0.0%	0.0%	100.0%
20	0.0%	0.3%	32.6%	29.2%	19.8%	9.1%	6.8%	1.4%	0.6%	0.3%	0.0%	100.0%
21	0.0%	0.0%	29.4%	32.0%	15.1%	12.3%	7.1%	3.1%	0.6%	0.3%	0.0%	100.0%
22	0.0%	0.0%	32.0%	26.6%	18.9%	12.0%	7.4%	2.0%	0.9%	0.3%	0.0%	100.0%
23	0.0%	0.3%	32.3%	30.7%	15.3%	11.7%	4.3%	4.3%	1.0%	0.0%	0.0%	100.0%
24	0.0%	0.0%	41.1%	23.0%	15.1%	12.1%	5.1%	2.1%	1.2%	0.3%	0.0%	100.0%
Grand Total	0.0%	0.1%	33.6%	27.8%	16.7%	11.5%	6.6%	2.5%	0.9%	0.2%	0.1%	100.0%

Area Fraction BinNum												
Sample	-1	1	2	3	4	5	6	7	8	9	10	Grand Total
(blank)	#DIV/0!	#DIV/0!	#DIV/0!	#DIV/0!	#DIV/0!	#DIV/0!	#DIV/0!	#DIV/0!	#DIV/0!	#DIV/0!	#DIV/0!	#DIV/0!
1	0.0%	0.0%	1.3%	3.2%	4.1%	13.5%	28.6%	25.7%	23.5%	0.0%	0.0%	100.0%
2	0.0%	0.0%	0.6%	1.3%	2.3%	7.6%	11.3%	14.3%	30.5%	0.0%	32.2%	100.0%
3	0.0%	0.0%	1.6%	3.7%	7.7%	22.6%	28.3%	25.6%	10.6%	0.0%	0.0%	100.0%
4	0.0%	0.0%	1.0%	1.9%	3.3%	8.2%	17.9%	5.7%	20.3%	41.7%	0.0%	100.0%
5	0.0%	0.0%	1.2%	2.7%	5.3%	6.7%	16.9%	23.8%	9.3%	0.0%	34.1%	100.0%
6	0.0%	0.0%	1.4%	3.8%	6.7%	7.7%	20.6%	19.6%	40.3%	0.0%	0.0%	100.0%
7	0.0%	0.0%	0.8%	1.6%	2.9%	4.4%	8.5%	14.7%	15.7%	0.0%	51.4%	100.0%
8	0.0%	0.0%	1.7%	4.0%	5.5%	15.7%	14.4%	36.3%	0.0%	22.4%	0.0%	100.0%
9	0.0%	0.0%	0.7%	1.1%	2.0%	5.1%	8.6%	12.2%	18.8%	0.0%	51.5%	100.0%
10	0.0%	0.0%	1.0%	2.1%	3.9%	9.7%	14.3%	16.7%	36.4%	15.8%	0.0%	100.0%
11	0.0%	0.0%	0.6%	1.0%	2.8%	4.2%	9.8%	10.9%	14.1%	10.8%	45.9%	100.0%
12	0.0%	0.0%	0.7%	1.4%	5.0%	10.6%	19.4%	27.5%	35.4%	0.0%	0.0%	100.0%
13	0.0%	0.0%	0.7%	1.8%	4.3%	8.1%	12.9%	22.0%	50.3%	0.0%	0.0%	100.0%
14	0.0%	0.0%	0.7%	1.5%	2.2%	7.5%	13.1%	4.8%	12.5%	0.0%	57.6%	100.0%
15	0.0%	0.0%	1.1%	2.7%	5.9%	12.2%	16.9%	28.7%	16.3%	16.2%	0.0%	100.0%
16	0.0%	0.0%	1.1%	2.3%	3.3%	9.2%	15.7%	26.1%	0.0%	42.2%	0.0%	100.0%
17	0.0%	0.0%	1.2%	4.1%	7.4%	18.3%	33.1%	35.8%	0.0%	0.0%	0.0%	100.0%
18	0.0%	0.0%	0.6%	2.0%	3.7%	8.2%	16.5%	12.1%	30.1%	26.8%	0.0%	100.0%
19	0.0%	0.0%	1.3%	2.6%	5.8%	14.7%	21.6%	20.0%	34.1%	0.0%	0.0%	100.0%
20	0.0%	0.0%	1.4%	3.4%	7.0%	10.2%	22.7%	12.4%	13.7%	29.2%	0.0%	100.0%
21	0.0%	0.0%	0.9%	2.7%	4.3%	10.8%	21.8%	28.8%	15.9%	14.9%	0.0%	100.0%
22	0.0%	0.0%	1.0%	2.4%	5.3%	11.4%	22.0%	15.5%	27.3%	15.1%	0.0%	100.0%
23	0.0%	0.0%	1.2%	3.0%	5.0%	11.3%	15.2%	40.6%	23.6%	0.0%	0.0%	100.0%
24	0.0%	0.0%	1.3%	2.0%	4.1%	10.4%	12.4%	13.6%	28.8%	27.5%	0.0%	100.0%
Grand Total	0.0%	0.0%	1.0%	2.2%	4.1%	9.2%	16.0%	18.3%	21.1%	10.7%	17.5%	100.0%

Size Distributions

Count of Area	Eq. Diam											
	1.78	5.62	10.00	17.79	31.63	56.25	100.02	177.87	316.30	562.47	1000.23	
	BinNum											
Sample	-1	1	2	3	4	5	6	7	8	9	10	Grand Total
(blank)	0	0	0	0	0	0	0	0	0	0	0	0
1	0	0	94	81	34	35	28	5	3	0	0	280
2	0	0	98	83	46	46	25	12	6	0	1	317
3	0	0	84	80	44	42	20	6	1	0	0	277
4	0	1	168	118	65	46	37	4	5	2	0	446
5	0	2	184	153	99	41	32	16	2	0	1	530
6	0	0	129	132	79	26	23	8	4	0	0	401
7	0	2	172	121	79	32	22	11	4	0	1	444
8	0	1	144	120	55	48	13	11	0	1	0	393
9	0	2	96	56	31	25	15	6	3	0	1	235
10	0	1	140	107	62	52	23	9	6	1	0	401
11	0	0	109	73	64	33	24	8	3	1	1	316
12	0	0	83	58	56	41	22	11	5	0	0	276
13	0	0	61	55	44	27	14	8	4	0	0	213
14	0	0	137	115	54	55	29	4	3	0	1	398
15	0	0	130	113	79	53	23	13	3	1	0	415
16	0	0	107	84	37	33	19	8	0	2	0	290
17	0	0	70	81	45	35	22	7	0	0	0	260
18	0	0	61	80	47	32	21	5	4	1	0	251
19	0	1	143	107	74	57	29	8	4	0	0	423
20	0	1	115	103	70	32	24	5	2	1	0	353
21	0	0	103	112	53	43	25	11	2	1	0	350
22	0	0	112	93	66	42	26	7	3	1	0	350
23	0	1	97	92	46	35	13	13	3	0	0	300
24	0	0	136	76	50	40	17	7	4	1	0	331
Grand Total	0	12	2773	2293	1379	951	546	203	74	13	6	8250

Particle Area	BinNum											
Sample	-1	1	2	3	4	5	6	7	8	9	10	Grand Total
(blank)	0.0	0.0	0.0	0.0	0.0	0.0	0.0	0.0	0.0	0.0	0.0	0.0
1	0.0	0.0	4889.2	11692.2	15146.2	49458.6	104973.3	94401.3	86419.8	0.0	0.0	366980.5
2	0.0	0.0	5256.8	11686.4	20858.1	69756.6	104045.6	131415.0	280204.9	0.0	296343.0	919566.4
3	0.0	0.0	4370.0	10367.8	21365.7	62988.6	79015.8	71425.2	29434.8	0.0	0.0	278968.0
4	0.0	23.3	8669.9	16464.8	28909.7	71308.5	155196.2	49878.6	176188.5	361828.7	0.0	868468.3
5	0.0	46.7	9335.1	21552.4	42428.1	53711.9	135580.8	190459.5	74360.0	0.0	273244.4	800718.8
6	0.0	0.0	6662.9	18786.9	33110.5	37678.8	101285.9	96513.3	198149.3	0.0	0.0	492187.7
7	0.0	46.7	9078.4	18162.6	32626.2	49674.4	96490.0	166695.8	177367.0	0.0	581197.9	1131339.1
8	0.0	23.3	7491.4	17141.6	23658.7	67574.5	61944.3	156188.0	0.0	96676.7	0.0	430698.5
9	0.0	46.7	5029.3	8034.0	15006.2	38133.9	64149.7	91011.5	140160.8	0.0	383416.2	744988.2
10	0.0	23.3	7164.7	15181.2	27690.3	68992.3	101379.3	117984.1	257929.0	112073.8	0.0	708417.9
11	0.0	0.0	5688.6	10432.0	29370.6	42918.2	100865.8	112167.1	145656.8	111472.8	473855.8	1032427.8
12	0.0	0.0	4060.8	7713.1	27270.2	58105.2	106344.4	150616.1	193849.3	0.0	0.0	547959.1
13	0.0	0.0	3121.4	8144.9	19242.0	36453.6	58035.2	98969.6	226294.7	0.0	0.0	450261.4
14	0.0	0.0	7281.4	15694.7	23226.9	78280.7	136537.6	49738.6	129921.4	0.0	599226.3	1039907.5
15	0.0	0.0	6692.1	16418.1	36307.7	74908.4	103917.2	176486.0	100095.7	99763.1	0.0	614588.4
16	0.0	0.0	5536.9	11838.1	16651.5	46868.1	79692.6	132581.9	0.0	214334.1	0.0	507503.1
17	0.0	0.0	3547.3	11651.4	21015.7	52154.1	94068.7	101939.4	0.0	0.0	0.0	284376.5
18	0.0	0.0	3179.8	11639.7	21330.7	46751.4	94424.6	69663.2	172588.6	153813.4	0.0	573391.4
19	0.0	23.3	7182.2	14866.2	32748.7	83321.7	122715.8	113859.1	193756.0	0.0	0.0	568473.0
20	0.0	23.3	5898.6	14282.7	29533.9	43244.9	95725.7	52492.5	57982.7	123170.9	0.0	422355.2
21	0.0	0.0	5163.5	14877.8	23915.4	60199.8	121980.7	160873.1	88946.1	83350.8	0.0	559307.1
22	0.0	0.0	5723.6	13226.7	29358.9	63268.7	122552.5	86501.4	152022.2	83870.1	0.0	556524.0
23	0.0	23.3	5005.9	12981.6	21313.2	48653.4	65514.9	174642.3	101636.0	0.0	0.0	429770.8
24	0.0	0.0	6966.4	11318.8	22602.6	57603.4	68519.7	75036.8	159093.6	151893.9	0.0	553035.1
Grand Total	0.0	280.1	142995.9	324155.8	614687.6	1362009.6	2374956.2	2721539.6	3142056.9	1592248.3	2607283.7	14882213.6

Count Distribution

Area Distribution